2014-07-10

Deconvolution of High Rate Flicker Electroretinograms

Ahmad O. Alokaily
University of Miami, aalokaily@ksu.edu.sa

UNIVERSITY OF MIAMI

DECONVOLUTION OF HIGH RATE FLICKER ELECTRORETINOGRAMS

By

Ahmad Alokaily

A THESIS

Submitted to the Faculty
of the University of Miami
in partial fulfillment of the requirements for
the degree of Master of Science

Coral Gables, Florida

August 2014

UNIVERSITY OF MIAMI

A thesis submitted in partial fulfillment of
the requirements for the degree of
Master of Science

DECONVOLUTION OF HIGH RATE FLICKER ELECTRORETINOGRAMS

Ahmad Alokaily

Approved:

_____ Jorge Bohorquez, Ph.D. Associate Professor in Practice of Biomedical Engineering	_____ Ozcan Ozdamar, Ph.D. Professor of Biomedical Engineering, Otolaryngology, Pediatrics, and Neuroscience
_____ Vittorio Porciatti, Ph.D. Research Professor of Ophthalmology	_____ M. Brian Blake, Ph.D. Dean of the Graduate School

ALOKAILY, AHMAD (M.S., Biomedical Engineering)
Deconvolution of High Rate Flicker Electroretinograms (August 2014)

Abstract of a thesis at the University of Miami.

Thesis supervised by Professor Jorge Bohorquez.
No. of pages in text. (70)

Flicker electroretinograms are steady-state electroretinograms (ERGs) generated by high rate flash stimuli that produce overlapping periodic responses. When a flash stimulus is delivered at low rates, a transient response named flash ERG (FERG) representing the activation of neural structures within the outer retina is obtained. Although FERGs and flicker ERGs are used in the diagnosis of many retinal diseases, their waveform relationships have not been investigated in detail. This study examines this relationship by extracting transient FERGs from specially generated quasi steady state, random ERGs at stimulation rates above 10 Hz and similarly generated conventional flicker ERGs. The ability to extract the transient FERG responses by deconvolving flicker responses to temporally jittered stimuli at high rates is investigated at varying rates. FERGs were obtained from seven normal subjects stimulated with LED-based displays, delivering steady state, low jittered quasi steady state and low jittered random responses at five stimulation rates of 10, 15, 32, 50, 68 Hz. The two deconvolution methods (CLAD and RAD) enabled a successful extraction of "per stimulus" unit transient ERG responses for all high stimulation rates. The deconvolved FERGs were used successfully to synthesize flicker ERGs obtained at the same high stimulation rates. The experimental results showed that, as the

stimulation rate increased, the a-wave and b-wave amplitudes decreased significantly between the 10 and 15 Hz and 15 and 32 Hz. Furthermore, the implicit time of a-wave increased between 2 and 10 Hz and decreased between 15 and 32 Hz. Moreover, b-wave decreased significantly as the stimulation rate increased up to 32 Hz.

Acknowledgments

I would like to express appreciation and thanks to my advisor Dr. Jorge Bohorquez for the marvelous academic advising during my master degree and encouraging my research. I would also like to thank my committee members, Dr. Ozcan Ozdamar, and Dr. Vittorio Porciatti for joining my master thesis committee. My sincere gratitude is also extended to Juan Manuel Lopez and Mohamed Almadi for their help in programing and editing respectively. A special thanks to my parents and Tariq Alzaied who supported me morally during my study. At the end I would like to thank all the volunteers for participating in this study.

TABLE OF CONTENTS

LIST OF TABLES

LIST OF FIGURES

Chapter 1

Introduction

Electrophysiology is the study of the electrical nature of biological cells and tissues. It is the basis of several ophthalmological techniques that can provide information about the retinal function. Three distinct electrical potentials have been identified in retina are early receptor potential (ERP), electroretinogram (ERG), and electrooculogram (EOG). ERP is generated by the photoreceptors in the outer retina. ERG generation extends from pigment epithelium to the inner nuclear layer. EOG is a function of pigment epithelium but also depends on outer and inner layers of the retina.

ERG arises in the retina after light stimulation and is detectable all around the eye. The light stimuli may either be a pattern (spatially structured) or flash (unstructured) and the retina may be partially or fully stimulated. However, the electrical potential is largest at the center of the cornea. It results from the composite activity of millions of retinal cells. Since all the cells in the inner and outer nuclear layer of the retina contribute to ERG, it can be used as a function of these cells. The magnitude and the shape of ERG depend upon the amount of light reaching the retina. If the retina is strongly illuminated, the ERG is large and fast changing and vice versa. The rods and cones contribute their signals to the ERG in an independent way. One can separate the responses from the rods and cones in human ERG by the differences in their wavelength sensitivity and behavior to light adaptation and flicker (Gauras, 1970).

The ERG consists of a negative deflection (a-wave) and a positive deflection (b-wave). A-wave is due to the response of photoreceptors and is generally not recordable in rod ERG responses in case of low intensity flashes. B-wave is associated with on-bipolar cell function and is recorded in lower intensity flashes that do not produce the a-wave

response. ERG is utilized in the detection of hereditary retinal disorders such as retinitis pigmentosa, pigmentary retinopathies, cone dystrophies, juvenile X-linked retinoschisis, congenital stationary night blindness and macular disorders. Though ERG is an important clinical tool, it has limited use in evaluation of abnormalities involving very small areas of the retina such as fovea. The limitation is due to the fact that large areas of retina must be illuminated in order to produce a detectable ERG response (Gundogan et al., 2011).

Full-field ERG is the diffuse response of both neural and non-neural retinal cells to a light stimulus. This response is the sum of both the positive and negative components originating from different stages of retinal processing. The electrical activity in the ERG results from light-induced changes in the trans-retinal movements of sodium and potassium ions in the extracellular space. In many studies, the electrical retinal responses are recorded by electrodes that contact the cornea or the bulbar conjunctiva. These electrodes may be of several types such as contact lens electrodes, conductive fibers and foils, conjunctival loop electrodes, corneal wicks (Gundogan et al., 2011).

Recently, surface electrodes placed on lower eyelids are used to record the electrical retinal responses in different studies with satisfying reported results. (Porciatti & Ventura, 2004; Papathanasiou & Papacostas, 2008)

There are several specialized types of ERGs that provide additional information about retinal function. These include macular/focal ERG, pattern ERG, multifocal ERG, direct-current ERG, bright flash and double flash ERG, etc. (Marmor et al, 2004). Pattern electroretinogram (PERG) is a specific type of ERG that represents retinal response induced by contrast reversing pattern. It aids in the functional assessment of retinal ganglion cells and finds use in the investigation of anterior visual pathway disease. It

provides valuable information about macular functions; however, it lacks the topographical information of the retinal response. The conditions like optic neuritis, glaucoma and optic atrophy have reduced or completely absent PERGs in the presence of intact ERGs (Holder, 1987; Porciatti et al., 2013). Multi-focal electroretinography (mfERG) is another technique for the analysis of local retinal function. It enables topographic mapping of retinal function in the central 40-50 degrees of the retina (Hood et al., 2012).

One of the most important techniques that measure the electrical potential of the retina in response to full flash stimuli is flash electroretinography (FERG). Rapid changes in the retinal electrical potential take place after the stimulation with a uniform light flash. These changes lead to the generation of a flash electroretinogram. The formation of the waves during stimulation evokes activity from the outer retinal layers. These waves are indicative of the functional condition of retinal layers. By controlling the stimulus' frequency, the FERG responses can be categorized into transient response at low frequency stimulation and steady state response at high stimulation rate. In the steady state response resulting from the overlapping of the transient ERG responses, the important temporal information is lost (Heinrich, 2010).

The present study aimed at extracting the per-stimulus transient response evoked by the retina in response to high-stimulation rate stimuli in order to be able to analyze the temporal component of the FERG accurately in real time. Anatomy and physiology of the visual system have been discussed in the beginning (chapter 2) of the thesis so as to make the process of the vision clear. The electrophysiology of the vision is also discussed along with the different types of electroretinographies. Chapter 3 of the thesis presents the

methods used in the study. It focuses the instrumentation, recording and processing of the data. The results and discussion of the study have been summarized in chapters 4 and 5 respectively. In this study, two different mathematical theories were used to study the ability of extracting the per-stimulus transient response evoked by the retina in response to high-stimulation rates and compare their capability to provide consistent and dependable results. Overall, this study will provide more reliable information for understanding the sources of retinal disorders.

Chapter 2

Background

2.1 Anatomy and Physiology of the Visual System

The human visual system has the capacity to detect only specific range wavelengths within the electromagnetic spectrum. The wavelengths that can be detected by the eye range from 400nm to about 700nm. This portion of the electromagnetic spectrum is known as visible light. Thus, the human eye cannot detect other wavelengths, such as ultraviolet or infrared, which are outside of this range. The wavelengths within the visible light act as the visual stimulus to the eye, which provides the link between the physical world and the conceptual world. Each wavelength provides a given level of stimulation, which plays a crucial role in determination of different colors that people experience. Visual processing is a complex task that highly organized and efficient computational capacity from the brain. In order to meet these demands, there is a highly organized and efficient neural system. Scientists have tried to uncover and understand the complex pathways and networks forming the visual system. They have developed an anatomy of the visual system that enables detailed localization of neuropathological processes. Furthermore, it has provided a guide to development of effective diagnosis and therapy of neuro-ophthalmic disorders (Rogers, 2011).

The process of receiving, transmitting, and processing of visual signals is performed by the visual pathways. The visual pathway is a complex structure consisting of the eye, optic nerves, lateral genital geniculate nucleus (LGN) of the thalamus, optic tracts, chiasm, extrastriate cortices, and striate cortex. The mechanism of processing visual signals is formed by the functioning and anatomical relationships between these parts. This section will describe the anatomy and then physiology of the visual system. It

will examine these structures in detail in order to understand how they are organized and coordinated for proper functioning.

2.1.1 The Eye

The eye is the main sensory organ for vision. Its purpose is to gather light, focus it, and generate neural signals of the visual pathway, which transmits them to the brain for interpretation. Figure 2.1 below shows the structure of the eye.

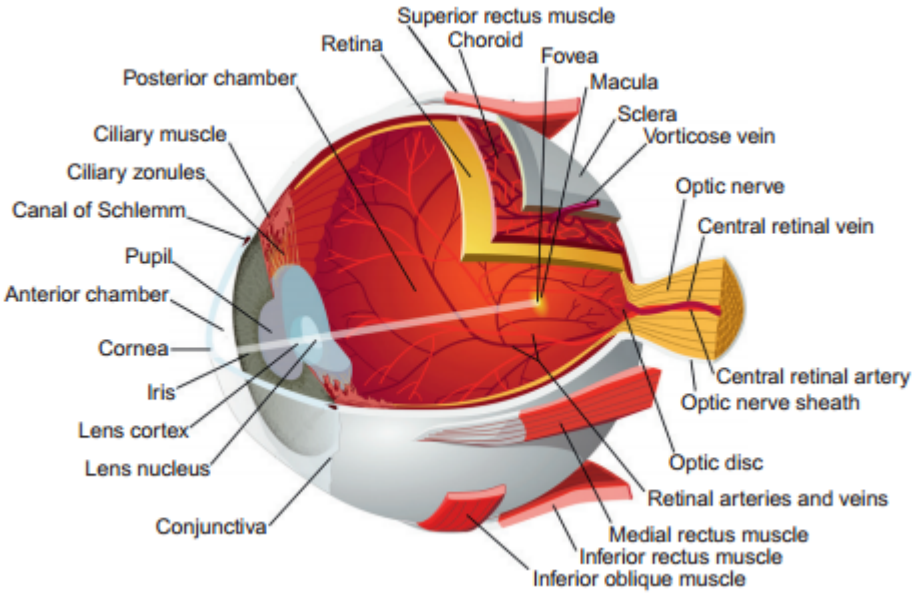

Figure 1.1: The structure of the eye (Prasad & Galetta, 2011)

As shown in the diagram above, the eye is made up of many parts. For easy description of the eye, its structure is divided into various parts. These parts include the protective structures, anterior segment, posterior segment, and the visual system pathways to the brain.

2.1.1.1 Protective Structures

The protective structures of the eye include the orbit, lids, and the sclera. The orbits are located in front of the scull to provide physical support and protection to the eye. It is wide at the front and leaves a narrow opening at its rear end, which provides an

exit for the optic nerve that links the visual pathways to the brain. The eyelids are cartilage-like tarsal plates that provide protection to the eye. They also contain tear glands, row of cilia, and eyelashes, which provide further protection to the eye. The sclera is a thick, opaque white tissue that covers most of the surface area of the eye (Prasad & Galetta, 2011).

2.1.1.2 The Anterior Segment

The anterior segment of the eye is composed of the cornea, aqueous humor, iris, crystalline lens, and the ciliary muscles.

The cornea is a transparent tissue that is dome shaped and located at the front of the eye. The transparence is very low at the edge of the cornea, where it integrates to the opaque sclera. In order to provide proper functionality, the cornea is more curved than the rest of the globe. Its structure is composed of evenly distributed collagen fibrils, which are organized in a crisscrossed manner to cover the whole of the cornea to form a layer called the stroma. The purpose of this layer is to provide transparence and strength to the cornea. The primary purpose of the cornea is to transmit and focus light into the retina of the eye. The curvature of the cornea gives it the ability to focus light into the retina (Roberts, 2010).

Apart from the stroma, the cornea is composed of four other layers. The first layer, epithelium, is used to protect the cornea from bacteria or other pathogens. It consists of tight cell junctions which help the stroma to maintain the required level of hydration. The second layer, Bowman's layer, is located beneath the epithelium. It is a thin membrane that provides protection to the stroma of the cornea. The third layer is a thin membrane, Descemet's membrane, which also protects the cornea. The last layer, the endothelium, is a thin layer of cells that allows nutrients from the aqueous humor into the

cornea and waste products out of the cornea. It coordinates with the epithelium to maintain the required level of hydration so as to maintain the transparency of the cornea. Lack of proper hydration may affect the arrangement of the corneal fibrils, and increase the scattering of light.

The aqueous humor is a fluid that fills the anterior chamber of the eye. The anterior chamber of the eye is located between the cornea and the front surface of the crystalline lens. It is produced by the ciliary body. The aqueous humor serves two functions in the structure of the eye. Its first function is to provide nutrients to the cornea and the crystalline lens, since it is essentially a fortified blood plasma. The aqueous humor is also an optical pathway of the eye. It plays an important role in focusing the light into the retina as a result of its refractive properties. The refractive index of the aqueous humor is about 1.333, while that of the cornea is about 1.376. The lens of the eye has a refractive index gradient which ranges from 1.406 to 1.386. The differences in the refractive indices makes light to bend at the interfaces surrounding the aqueous humor (Remington, 2012).

The iris is located after the cornea and its purpose is to regulate the amount of light entering the eye. The center of the iris contains an opening at the middle, called the pupil. The iris controls the amount of light entering the eye by either dilating or constricting the pupil. When there is too much light entering the eye, the iris constricts the pupil thereby allowing less light to enter. When there is less light that is entering the eye, the iris dilates the pupil to allow more to enter. The iris uses circular muscles, sphincter muscles to constrict the pupil and radial muscles, dilator muscles to dilate it. The iris pigmentation at the anterior layer gives the eye its color (Bear et al., 2007).

The crystalline lens is a transparent structure consisting of regularly elongated fiber cells. The most important property of the crystalline lens is its ability to change its shape so as to regulate its refractive power. The purpose of increasing or decreasing its refractive power is to focus near or far objects. Its refractive index ranges from 1.38 to 1.41 (Remington, 2012). The fiber cells adjacent to the surface of the lens have a lower refractive index as compared to that of the deeper cells. The variations in curvature of the lens are brought about by the action of the ciliary muscles. The lens is pulled to its flattest curvature when the ciliary muscles are relaxed. This reduces the focal power of the lens, a condition called emmetropic, which enables the eye to focus a distant object. Contraction of the ciliary muscles allows the lens to take up its preferred round shape, thereby increasing its power to focus the nearby objects (Remington, 2012).

2.1.1.3 The Posterior Segment

The posterior segment of the eye is composed of the retina and the vitreous humor.

2.1.2 The Retina

The retina is located at the back of the eye and its purpose is to convert light energy into electrochemical signals, which are then relayed by neurons into the brain. It consists of transparent inner layers including the nerve fiber layer, ganglion cells, amacrine cells, and the bipolar cells. In order to reach the photoreceptors, light must pass through these layers. The photoreceptor layer is surrounded by another layer called the retinal pigment epithelium (RPE). The photoreceptors are then followed by the outer plexiform layer, the inner plexiform layer, the ganglion cells, and the glial cells (Marieb, 2006). The Figure 2.2 below shows a simple organization of the retina.

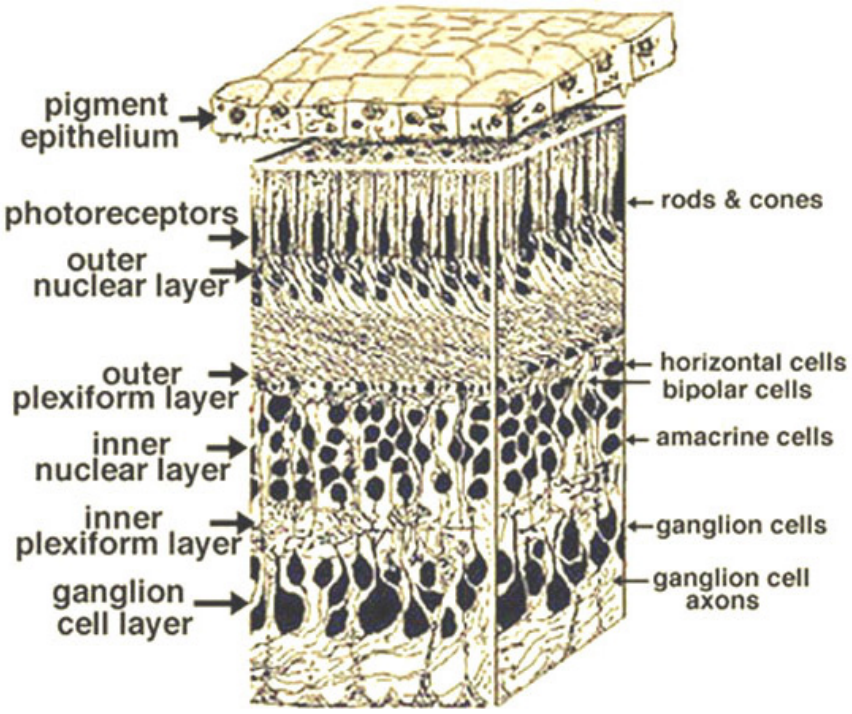

Figure 2.2: Organization of the retina (Kolb, et al., 2007).

The pigment epithelium (RPE) performs vitamin A metabolism, which provides metabolic and structural support to the photoreceptors. The first function of the RPE is light absorption due to its heavily pigmented cells. It absorbs the light that has been scattered, and in the process it improves the quality of the optical system. From the retinal side, the RPE is in contact with a robust photo-oxidative energy. On the other side near the choroid, the RPE is exposed to an overflow of oxygen. The photoreceptor outer segment tips require a steady renewal process from their base since the photo-oxidation process damages them.

The outer nuclear layer consists of the cell bodies of cones and rods. On the other hand, the inner nuclear layer consists of the cell bodies of the bipolar, horizontal, and amacrine cells. The ganglion cell layer consists of the cell bodies of the ganglion cells. The outer plexiform layer is a region which consists of the various synapses. These connections are those between rods and cones, and bipolar cells (vertically running) and

horizontal cells. The inner plexiform layer is a region that operates as a relay for nerve cells and bipolar cells to link to ganglion cells (Kolb et al, 2007).

There are four types of photoreceptors in the human eye, consisting of three cones and the rods. The cones have the capacity to function over a wider range of light intensities. Each type of cone photoreceptor can only be activated by a specific wavelength of light, and thus they give the eye the ability to differentiate between colors. On the contrary, the rods become saturated at natural light intensities, which make them lose the ability to differentiate between colors. They are highly sensitive, which makes them effective for night vision. The rods and the cones have different structures of opsin, which make them have different functionalities.

The rods have more photopigment as compared to the cones, and they are used for vision at low light levels. This condition is known as scotopic vision. They have a slow response due to long integration time. Rods do not have the capacity to detect color, and they have low visual acuity. Rods also have highly convergent retinal pathways and are not directionally selective.

The cones operate actively at higher light levels, a condition which can be described as photopic vision. There are three types of cones namely the S-cone, M-cones, and L-cones. The S-cones are short-wavelength sensitive cones, which actively detect the short-wavelength light waves. The M-cones are middle-wavelength sensitive cones, which are responsible for detecting light waves within the middle range of visible light. The L-cones are long-wavelength cones for detection of long-wavelength visible light. Cones have a fast response due to the short integration time. They also have less amplification, non-saturating response, and are directionally selective. The presence of

different types of cones to detect different wavelengths gives them the ability to detect different colors. There is a specific light level where all the cones become operational, a condition described as mesopic (Roberts, 2010).

The level of neural signal produced by the photoreceptor is dependent on the specific wavelength received and its intensity. The distribution of the photoreceptors, cones and rods, varies across the retina. This explains why the fovea and the retinal periphery have specialized functions. The fovea has a higher density of cones than the retinal periphery, which gives it the ability to provide excellent visual acuity. The retinal periphery has a high concentration of rods, which are virtually absent in the fovea. The neurosensory of the retina has three primary layers involved in the conversion of light energy into neurosensory signals. They include bipolar cells, the ganglion cells, and the amacrine cells. The photoreceptors synapse with the bipolar cells which are used to transmit information to the ganglion cells. The elements of these layers are connected through the amacrine cells (Hung & Ciuffreda, 2002).

2.1.3 Ganglion Cells

The ganglion cells collect visual messages from the retinal interneurons, the bipolar cells and the amacrine cells. They have synapses within their membranes, which allow them to receive the chemical messages from the retinal interneurons. The ganglion cell membranes, then, change the chemical information into intracellular electrical signals. The membrane receptors are integrated within the ganglion cell dendrites and cell body. The electrical signals, from the transmembrane receptors, are then digitalized into nerve spikes for transmission over long distances.

The ganglion cells form the most complex visual signal processing system in the retina. It is the detection efficiency of the ganglion cells that determine an organism can

behaviorally respond to different visual stimuli. Different ganglion cells are adapted to selectively detect specific characteristics of the visual scene. These features include color, shape, direction and speed of motion. The axons of the ganglion cells are connected and terminate in the brain. They usually terminate in the lateral geniculate nucleus (LGN) of the thalamus and the superior colliculus (Prasad & Galetta, 2011). The retinal ganglion cell provides a restricted region of visual space where light can stimulate electrical responses.

In the retina, the ganglion cells form the first neurons which respond with action potentials. The ganglion cell receptive field is divided into two receptive field sub-regions, center and surround. This forms two types of ganglion cell receptive fields, ON center/OFF surround and OFF center/ON surround. Under the ON center/OFF surround response, the response of the ganglion cell increases when a small bright spot is flashed in the center sub-region. The cell response is inhibited when a bright annulus is flashed in the surround sub-region. When a spot of light that covers both the center and the surround is flashed, there is little or no response since excitation at the center cancels the inhibition from the surround. The reverse takes place under the OFF center/ON surround. Under this condition, the cell response is inhibited by a small spot of light at the center while it is excited from an annulus in the surround. This is shown in Figure 2.3 and Figure 2.4 (Kolb et al., 2007).

2.1.4 The Visual Pathways to the Brain

The ganglion neurons are packed together to form an optic nerve. The optic nerve can consist of up to 1.2 million retinal ganglion cell axons (Marieb, 2006). The center of the optic nerve does not have any retinal photoreceptors, and thus, it does not have the ability to detect vision. The central point forms a depression commonly referred to as the

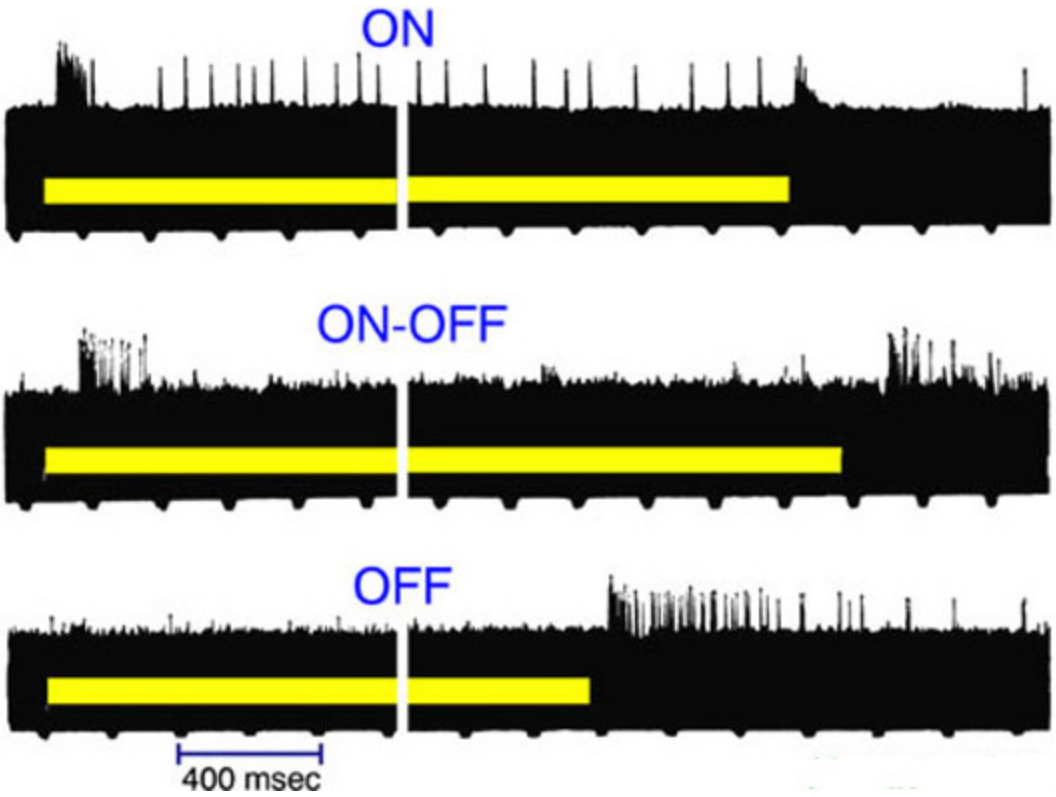

Figure 2.3: ON, OFF, and ON-OFF ganglion cells (Kolb et al., 2007).

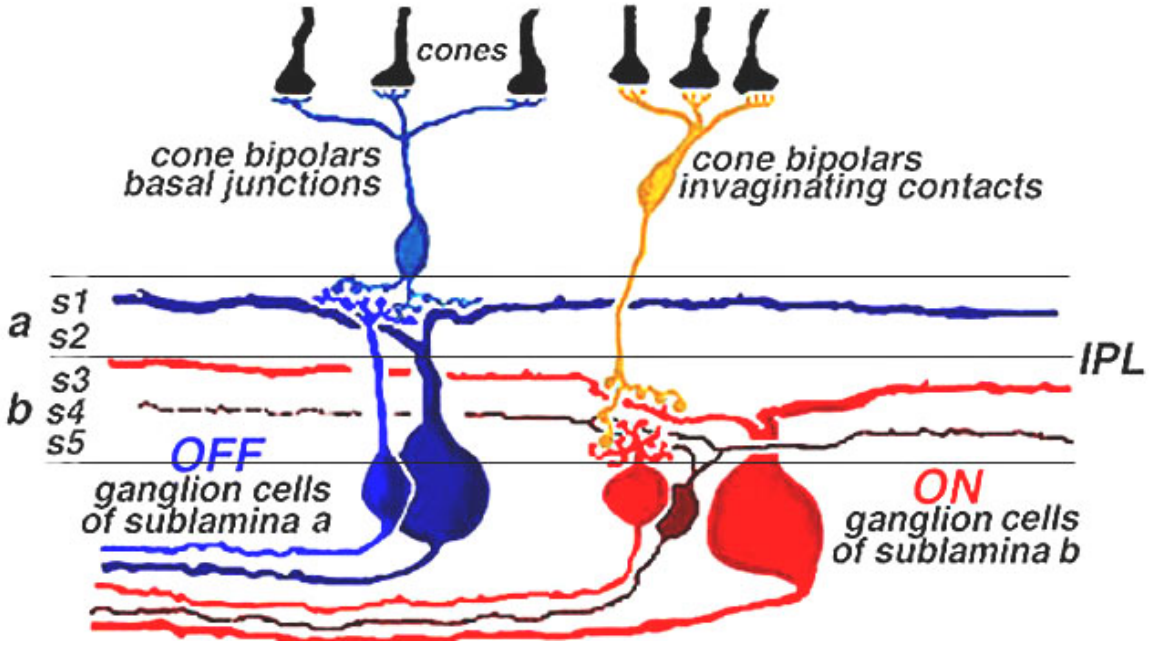

Figure 2.4: Organization of ON- and OFF-center ganglion cells (Kolb et al., 2007).

blind spot. The optic nerves of each eye are integrated at the optic chiasm, where about half of the axons of neurons from the retina cross to the opposite of the optic tract. Visual signals from the right side of the visual field reach the brain through the left optic tract and vice versa. At the end, each optic tract terminates at its lateral geniculate nucleus.

2.1.4.1 Thalamus

Visual information from the each half of the visual field is transmitted in separate pathways (Figure 2.5). The signals from the retinal ganglion cells travel to the lateral geniculate nucleus (LGN) of the thalamus.

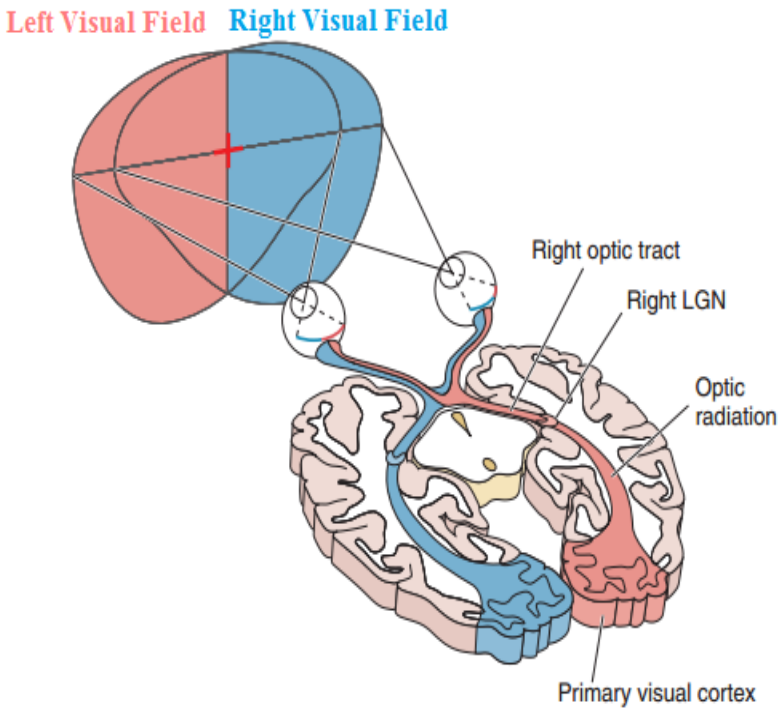

Figure 2.5: Human visual pathways (Modified from Bear et al., 2007).

The lateral geniculate nucleus is composed of six neuronal layers. The neural signals from each eye are maintained at separate layers. The LGN is a critical point in the visual pathway, since it has the dynamic ability to determine the amount and nature of messages that are relayed to the visual cortex. Furthermore, the LGN receives widespread restraining links from the thalamic reticular nucleus and layer six of the visual cortex.

2.1.4.2 The visual Cortex

The visual cortex refers to the occipital lobe of the brain that performs that final processing of the retinal signals. This is the place where the neural signals from the retina are processed leading to the occurrence of vision. The visual cortex is located at the most posterior section of the brain. It is divided into six different areas namely V1, V2, V3, V3a, V4, and V5 (Prasad & Galetta, 2011).

Area V1 is also known as the primary visual cortex. This is the first point where the neurons from the LGN form synaptic junctions. The primary visual cortex interprets the neural signals in terms of visual space. The visual space represents color, form, and orientation of the objects. The V1 area is mainly used to interpret neural signals originating from the fovea. The mapping of neural information from the fovea is known as cortical magnification. This process is common in primates and animals that depend on the information from the fovea for survival. The signals from the primary visual cortex are transmitted to the V2 area where further interpretation of form and color perception takes place.

The movement of neural signals further into the remaining areas of the visual cortex causes more associative processes to occur. Processes such as motion of the objects take place in sections of the visual cortex that create the parietal visual cortical areas. Interpretation of complex forms and patterns takes place in the temporal visual cortical areas, which include the middle temporal or V5 area. The interpretation of complex forms and patterns leads to recognition of objects (Rogers, 2011).

2.2 Electrophysiology of Vision system

ERG has many types of responses elicited by the retina. These response alternations are caused by the light stimuli being used during the procedure. Nonetheless,

the most specific types of ERG that have been under intensive research and commonly used in clinics are the pattern electroretinogram (PERG) and the flash electroretinogram (FERG).

2.2.1 The Pattern Electroretinogram

A retinal biopotential that arises from stimulating the human eye via temporally-patterned stimuli of constant mean luminance is called the pattern electroretinogram (PERG) (Figure 2.6). There are different kinds of stimulation patterns used in clinical practice to obtain PERG, such as a checkerboard display, or grating (Bach et al., 2013). Furthermore, the lack of a net change of stimulus luminance is the main cause that leads to the evoking of PERG. As shown in Figure 2.7, the pattern reversal of black and white stimuli stimulate the human's retina, leading to bright and dark responses that have the same magnitude but opposite signs that cancel each other revealing the uneven responses (Bach and Hoffman, 2006).

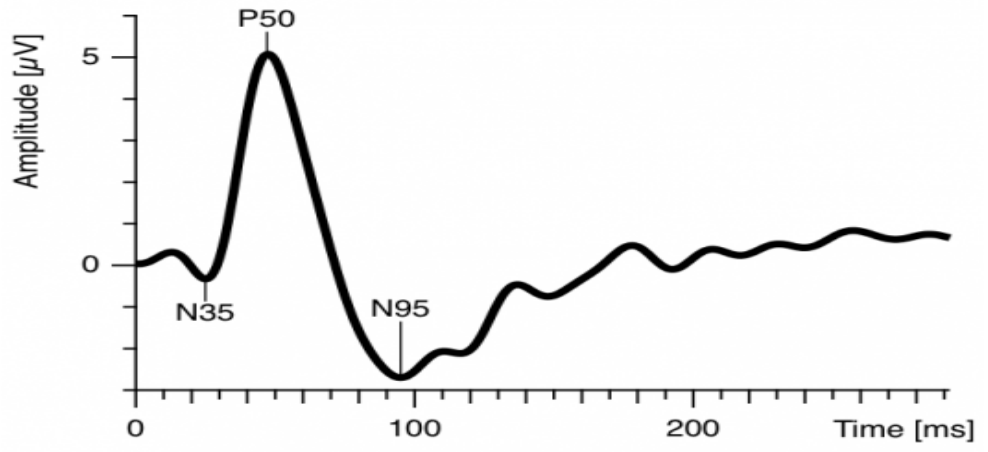

Figure 2.6: The standard transient response components of PERG (Bach et al., 2013).

As illustrated in Figure 2.6, the standard components of PERG are N35, P50, and N95. The amplitude of the PERG responses is typically in the range of 0.5-8 microvolts (Marmor et al., 1995). However, it has been shown that only P50 and N95 can be used in

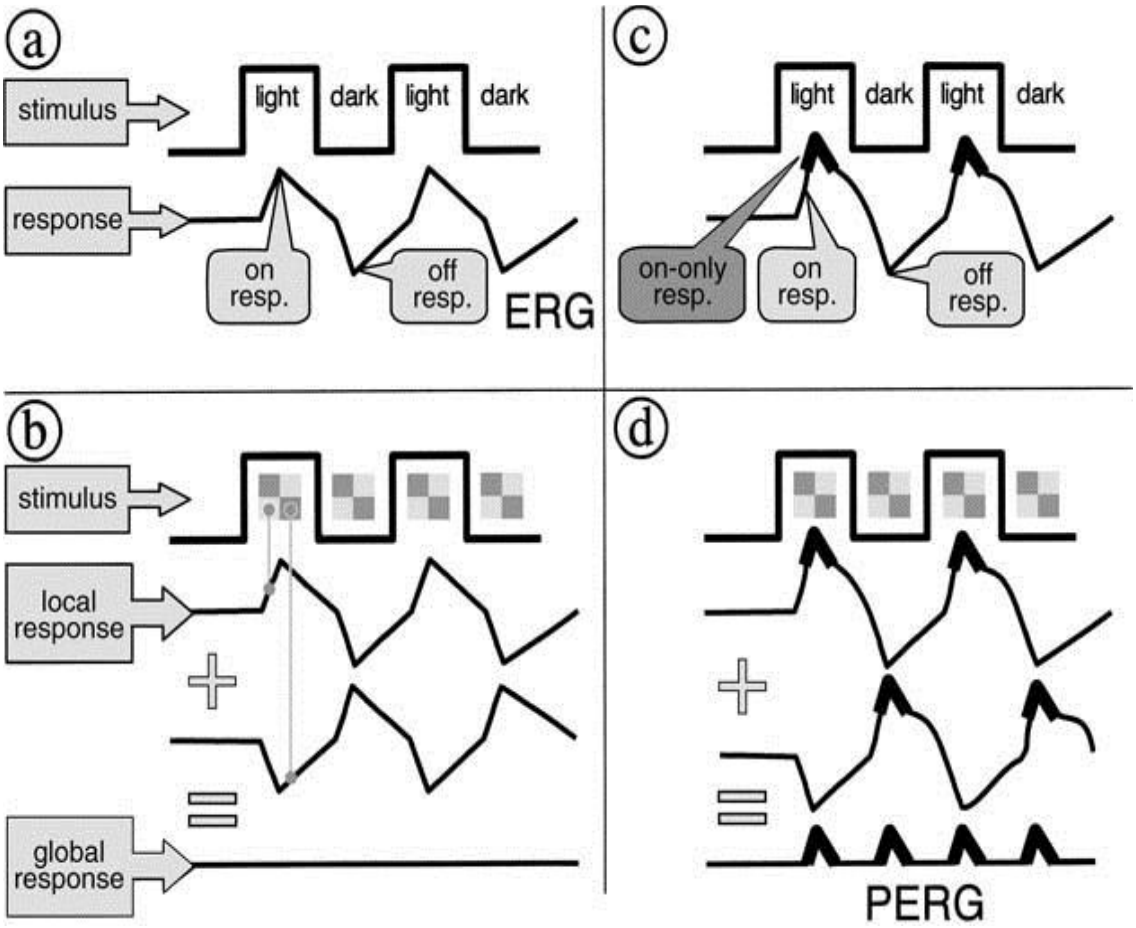

Figure 2.7: Nonlinear PERG response. (a) Illuminating the entire retina will cause an equal and opposite responses to both on response and off response. (b) In case of using pattern stimuli, the on response and off response is going to cancel each other giving no global response. (c) However, there exists a nonlinear on-only component. (d) PERG is a result of averaging the responses over the retina (Bach & Hoffmann, 2006).

real clinical practices. Recently, PERG has become a valuable biopotential diagnostic tool used in several clinical applications to detect various types of diseases that are related to any loss of ganglion cell activities (Bach & Hoffmann, 2006; Porciatti et al., 1987). For instance, studies have been conducted to examine the direct relation between the PERG changes and Glaucoma (Ventura et al., 2005; Porciatti & Ventura, 2009).

2.2.2 Flash Electroretinogram

The measurement of electrical potential of the retina in response to a full field flash stimulus is called the flash electroretinogram. Thus, changing the stimulus

characteristics results in different retinal responses. These retinal responses' differences in latencies and magnitudes from a flash light stimulus can reveal defects in the retina (Harden et al., 1989). Moreover, FERG responses are classified based on the experimental environments where a dark adaption procedure (Scotopic) focuses on the rods response and the light adaptation (Photopic) exposes the cones response to flash stimulus.

Nevertheless, to ensure consistency of ERG studies across the world, the International Society for Clinical Electrophysiology of Vision (ISCEV) has published standard protocols for ERG evaluation. The ISCEV states that depending on the adaption condition and the strength of the stimulus, the retinal responses differ accordingly (Figure 2.8). Based on that, the standard ERG responses are:

1. Dark-adapted 0.01($cd \cdot s \cdot m^{-2}$) ERG.
2. Dark-adapted 3.0 ($cd \cdot s \cdot m^{-2}$) ERG.
3. Dark-adapted 3.0 ($cd \cdot s \cdot m^{-2}$) oscillatory potentials.
4. Light-adapted 3.0 ($cd \cdot s \cdot m^{-2}$) ERG.
5. Light-adapted 3.0 ($cd \cdot s \cdot m^{-2}$) flicker ERG.

In a standard photopic FERG procedure (Figure 2.9), a-wave, b-wave and oscillatory potentials (OPs) are the main principle waves that are used clinically to assess the function of the retina. First, a-wave, negative peaks result from the hyperpolarization of the cone photoreceptors and OFF bipolar cells. After the a-wave, b-wave, positive peaks generated by Muller and ON bipolar cells. Then, OPs, with their ripple waveform, are believed to be evoked in the inner plexiform layer (Kim et al., 2010) (Figure 2.10).

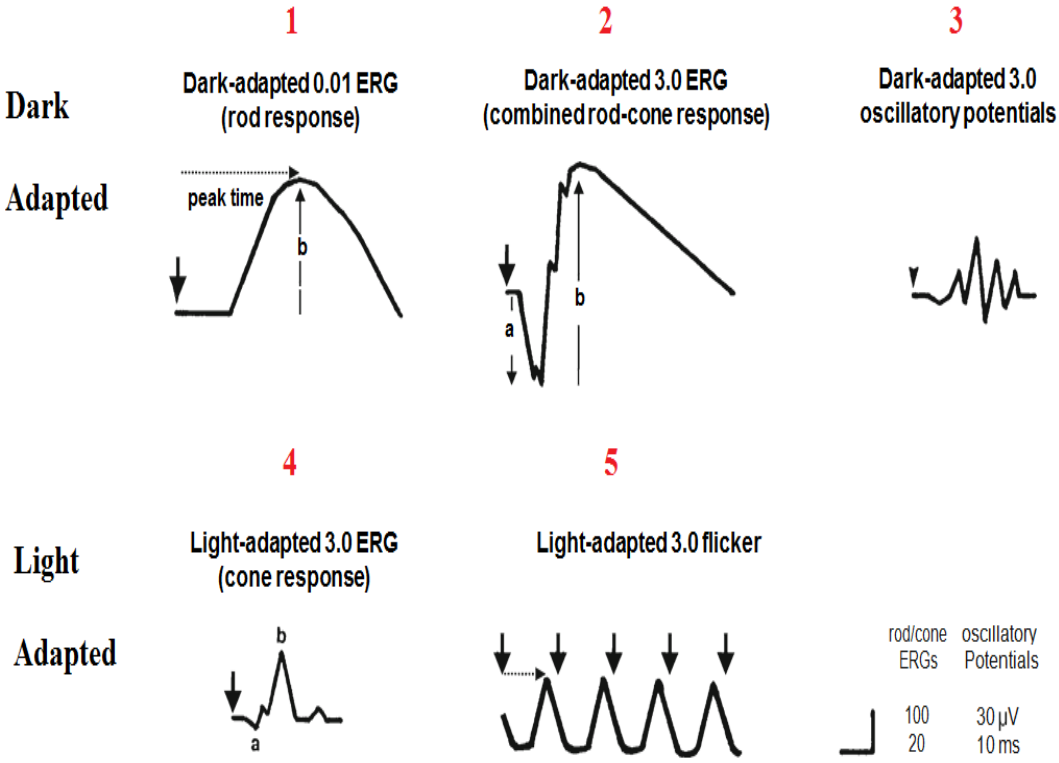

Figure 2.8: The standard ERG responses for different adaption conditions and flash strength. (1) Dark-adapted 0.01 ($cd \cdot s \cdot m^{-2}$) ERG. (2) Dark-adapted 3.0 ($cd \cdot s \cdot m^{-2}$) ERG. (3) Dark-adapted 3.0 ($cd \cdot s \cdot m^{-2}$) oscillatory potentials. (4) Light-adapted 3.0 ($cd \cdot s \cdot m^{-2}$) ERG. (5) Light-adapted 3.0 flicker ERG. The arrows represent the flash onset (modified from Marmor et al., 2009).

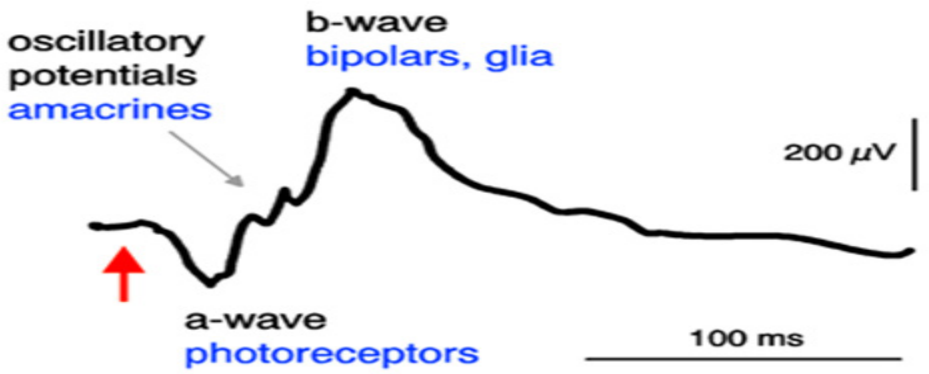

Figure 2.9: FERG standard photopic response. The onset of the stimulus is represented by the red arrow. The oscillatory potentials are generated by the amacrine cells. Cones and rods photoreceptors are response generate the a-wave. B-wave is evoked by the bipolar cells with the contribution of Müller cells (Modified from Niemeyer, 2001).

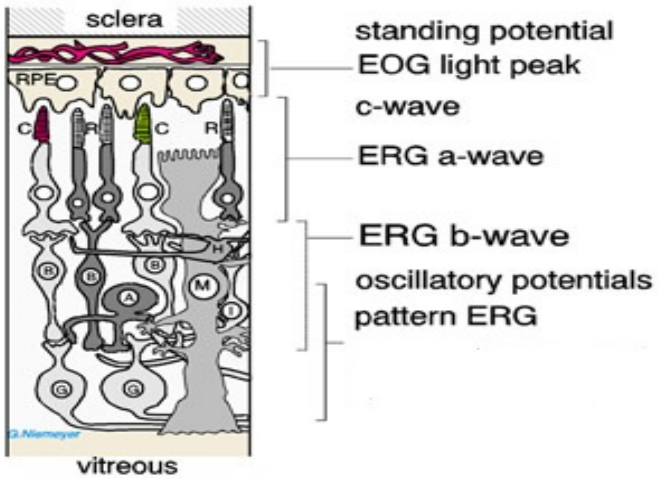

Figure 2.10: Photopic FERG wave origins. The exposure to light after dark adaption produces the ocular standing potential generated evoked by retinal pigment epithelium (RPE). The retinal photoreceptors, Cones (C) and rods (R), generate the negative a-wave potential. ON and OFF bipolar cell (B) with the contribution of the glial Müller cells (M) evoke the b-wave. The oscillatory potentials (OPs) of the ERG are generated by Interactions among amacrine cells (A). Ganglion cells (G) generate the pattern ERG (PERG) (Modified from Niemeyer, 2004).

In the case of the low frequency stimulus (less than 10 Hz), transient FERG components can be easily attained since all waves are resolved before applying the next stimulus. Accordingly, the FERG responses can be analyzed in the time domain depending on the magnitudes and the implicit times of the transient response (Toft-Nielsen, 2012). According to the ISCEV, the amplitude of the a-wave (a) is measured from the baseline to the a-wave negative peak, where the implicit times (latencies) of the a-wave (La) and the b-wave (Lb) are obtained from the flash stimulating onset to the peaks occurrence time. Also, the b-wave amplitude (b) is measured from the a-wave peak to the b-wave peak (see Figure 2.11) (Marmor et al., 2009).

Furthermore, when a high frequency isochronic stimulus is used (above 10 Hz), a convolved periodic response is generated (Figure 2.12). This resulted waveform is referred to as steady state or flickering ERG. Steady state ERGs occur as a result of using inter-stimulus intervals which are shorter than the ERG transient response. Consequently,

interpreting some ERG components in the time domain becomes very difficult. Therefore, steady state ERGs are analyzed in the frequency domain (Toft-Nielsen et al., in press).

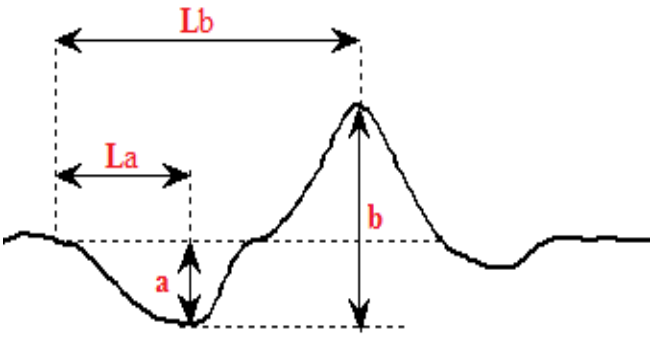

Figure 2.11: Latencies and amplitude temporal properties. (La): a-wave implicit time. (Lb): b-wave implicit time. (a) Negative potential a-wave. (b) Positive potential b-wave.

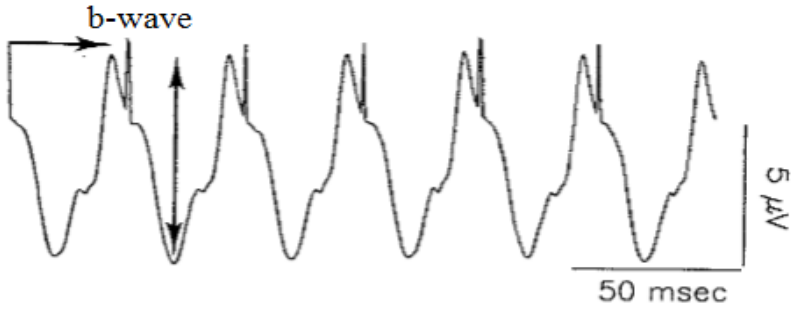

Figure 2.12: Standard Steady state ERG. Arrows shows the b-wave implicit time and magnitude. (Modified from Birch, 2006)

There are many factors that affect the generation of the ERG component. By relying on the reliability of the retina, and adjusting the flash stimuli properties and the ambient luminance, the ERG response alters (Asi & Perlman, 1991). For instance, as the frequency of the flash stimulus increases, the amplitude and the implicit time of the response decrease (Poppele & Maffei, 1967). Moreover, those differences enable researchers to isolate specific structures in the retina. This allows ophthalmologists to rely on the FERG as a clinical tool to diagnose cones and rod dystrophy, toxic retinopathy, retinitis pigmentosa, and retinal contribution in uveitis with opaque media,

and incomplete CSNB (Niemeyer & Stähli, 1996). However, there are many diseases and syndromes where the ERG responses become abnormal. These conditions may relate to either the cones or rods. Some of these conditions include degenerative myopia goldmann-favre vitreoretinopathy, ischemic central vein occlusion, Åland disease, and infantile Refsum's disease (Heckenlively et al., 2006).

2.3 Continuous Loop Averaging Deconvolution (CLAD)

As mentioned earlier, using stimulation sequences that have inter-stimulus intervals shorter than the transient response lead to response overlap (see Figure 2.13A). Thus, acquiring any transient evoked potential using conventional signal averaging techniques is restricted by using a stimulation sequence that must deliver the next stimulus after ensuring the completion of the previous response (Figure 2.13A). Otherwise, the resulted responses would overlap, and extracting a transient response for each stimuli would be impossible from the overlapped responses (see Figure 2.13B). Therefore, as a result of this limitation, the number of valid sequences and stimulation rates that can be used are limited (Delgado & Ozdamar, 2004).

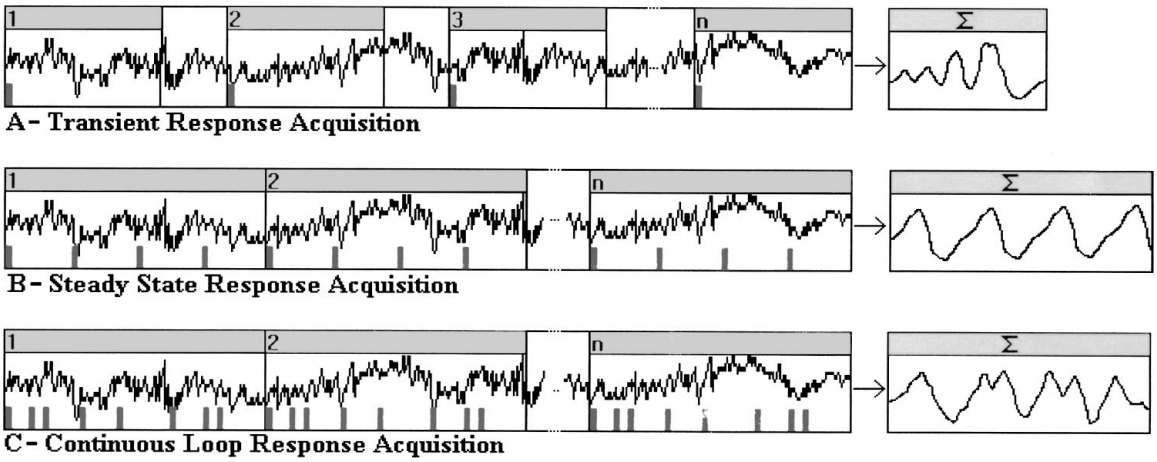

Figure 2.13: A – Conventional averaging transient response. B – Flickering (steady state) response acquired by conventional averaging methods. C – Complex response resulting from non-periodic sequence (Delgado & Ozdamar, 2004).

Continuous Loop Averaging Deconvolution (CLAD) is a mathematical theory intended to generate and deconvolve the output complex response (Figure 2.13C) that resulted from introducing non-isochronic sequences. These sequences differ from the regular steady state sequences by introducing periodic delays or advances (jittering) in the onset of stimuli. This method was first implemented by Delgado and Ozdamar (2004) in time domain and then modified into the frequency domain by Ozdamar and Bohorquez (2006). CLAD was developed primarily based on the assumption that the complex measured response is an arrhythmic sum of overlapped discrete responses. Moreover, every single response for each stimulus is independent from all other responses and has the same wave shape. Taking that into consideration, CLAD is able to deconvolve the complex response and give the per-stimulus transient response even when high-rate stimuli are used (Özdamar & Bohórquez, 2006)

At high stimulation rates, the deconvolution of evoked responses in time domain is introduced by using several simultaneous equations for a specific sequence. Then, these equations are solvable by algebraic matrices as long as the resulted matrix of coefficients is not singular. Based on the assumption that the evoked response is the same for each stimulus, there will be no adaption in the responses. So, the total acquired response, v(t), equals the superposition of all transient responses a(t)'s, resulting from number of stimulus presented, N.

$$v(t) = \int_{n-1}^{N} a(t - tn)$$

As the resulting response is a convolved signal, the above equation can be shown as:

$$v(t) = [M]\, a(t)$$

The M matrix vector is a diagonal representation of the stimulus sequence s(t) as values of ones and zeroes. In order to extract the per stimulus response a(t), the M matrix is inverted, yielding the possibility to get a(t) as the followed equation show:

$$a(t) = [M]^{-1}\, v(t)$$

Although CLAD was successfully able to deconvolve the convolved response to its per-stimulus transient response, there are still some issues in using it in the time domain. The deconvolution approach in time domain produces high unwanted noise, since in the time domain analysis does not allow the assessment of the noise amplification reduction characteristics. Consequently, this affects the results for some sequences. The solution for this issue was proposed by Ozdamar and Bohorquez (2006) by transferring the process from the time domain to the frequency domain (Ozdamar and Bohorquez, 2006).

Ozdamar and Bohorquez (2006) proved that in the time domain method, the overlapped response is presented as standard convolution of the stimulus sequence and the elementary response. Thus, using Fourier transformer to transform the measured response to the frequency domain changes the convolution into standard multiplication. Therefore, extracting the unitary response now is achieved by dividing the measured response by the stimulus sequence designed specially to not have zeroes as isochronic sequences as shown in equations below: (See Figure 2.14)

$$v(t) = a(t) * s(t) + n(t)$$

$$\Downarrow$$

$$V(f) = A(f)S(f)N(f)$$

$$\Downarrow$$

$$a(t) = FT^{-1}\left(\frac{V(f)}{S(f)} - \frac{N(f)}{S(f)}\right) \; if \; [S(f) \neq 0]$$

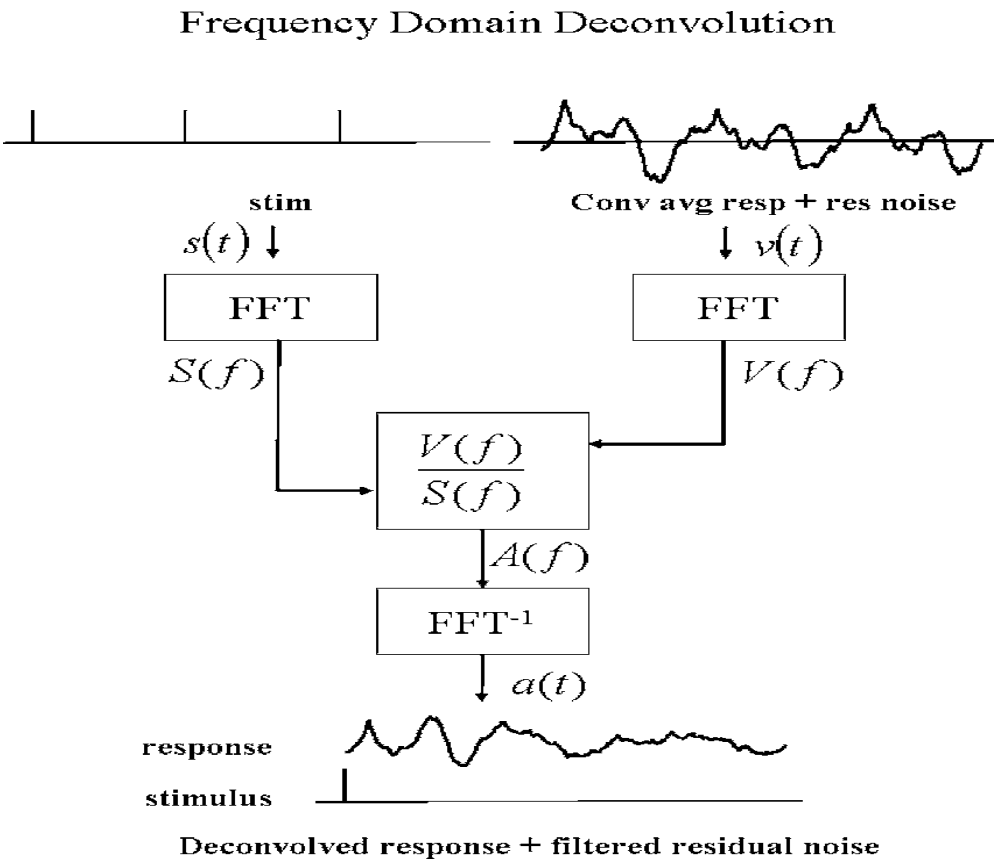

Figure 2.14:The convolution of the responses and sequence stimulus to the frequency domain to extract the per-stimulus response (Ozdamar & Bohorquez 2006).

Introducing the use of CLAD in frequency domain, Ozdamar and Bohorquez (2006) were able to identify the cause of the unwanted noise and reduce the computation time. However, designing CLAD sequences is a crucial step. Since generating non-zero sequences has a direct impact on the signals' quality represented by its signal-to-noise ratio (SNR), the sequences must be designed carefully to avoid any noise addition (Toft-Nielsen, 2012).

2.4 Random Averaging Deconvolution

Random Averaging Deconvolution (RAD) is a mathematical theory proposed by Bohorquez (2006) in an internal laboratory report that is under development. As CLAD allows the extraction of the per stimulus response stimulated by a using periodic

stimulation sequence, RAD on the other hand, enables the extrication of the per-stimulus response using an arbitrary stimulating sequence (Figure 2.15). Bohorquez proved that in experiments which use periodic stimulation sequences as CLAD sequences, subjects are able to perceive the sequence periodicity. To test the effect of "melody perception" on the acquired responses, a pseudo- non-periodic stimulating sequence, that has the similar histogram of periodic sequences, must be able to deconvolve the measured response to its per stimulus transient response. This sequence depends on the probability density function introduced by the histogram.

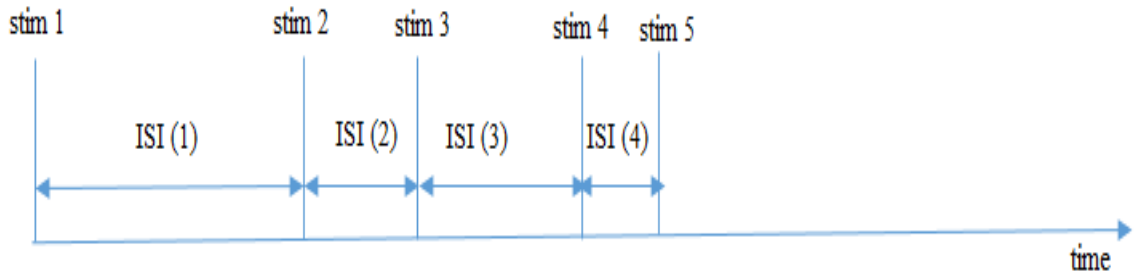

Figure 2.15: RAD stimulus sequence with random generated inter stimulus intervals (ISI).

As mentioned earlier, the evoked potentials a(j) with the length L are the same when a sequence, that has the same stimulus s(k), is used. Therefore, we can assume that the measured signal y(k) is a superposition sum of the evoked potentials $\hat{y}(k)$ plus noise e(k) as shown in equation 1:

$$y(k) = \hat{y}(k) + e(k) \quad (1)$$

where $\hat{y}$ can be presented as the convolution of stimulus and the evoked potential:

$$\hat{y} = a * s \quad (2)$$

so, based on minimizing the square error of the model, the evoked potential can be computed from the linear system matrix that depends only on the stimulus sequence. This

linear system is computed only once and then stored for effective deconvolution of the acquired signal. However, the approximation is needed when a long enough sequence is used. By using this approximation, constructing the matrix would be much faster with minimum and foreseeable transient response reconstruction error for long sequences.

In RAD, the stimulation sequence (s), the measured raw data (y), and the assumed response length (L) are the essential factors required in the deconvolution process. the implementation of this process can be summarized in four steps. The first step is to compute the first-length response values of the sequence autocorrelation. The second step is constructing the linear matrix system. Then, the first-response length L values of the cross-correlation between the sequence and the acquired signal are computed. Finally, the solution of the linear system can be found. Since the first two steps can be performed before acquiring the signals and storing them in the computer, RAD is considered a fast deconvolution method.

Recently, two deconvolution methods were proposed by different laboratories to extract the per stimulus auditory response using randomized stimulation similar to the RAD. In the first method, the overlapped evoked potentials were deconvolved by using the least square methodology. Using least square deconvolution allows the controlling amount of error by condition number of matrix associated with the low jittered stimulation sequence (Bardy et al., 2014). In another study, the auditory brainstem response (ABR) was recorded using the randomized stimulation and averaging method (RSA). RSA uses random inter-stimulation intervals that vary randomly as in RAD. RSA was able to deconvolve ABR responses successfully for rates higher than 100 Hz (Valderrama et al., 2012).

Chapter 3

Methods

3.1 The Population of the Study

In the study of full field electroretinogram, seven healthy adults (5 Males, 2 Females) with no known retinal diseases volunteered to participate. The subjects' ages were from 20 to 27, with an average age of 24.43 years. None of the participants wore eyeglasses or contact lenses. Before the subject's preparation, the goal of the study and the procedure was clearly explained. Also, subjects were given enough time to read and sign the consent forms in accordance with the Institutional Review Board of the University of Miami. All subjects were seated in an isolated chamber to eliminate any electrical interference that may cause noise or signal degradation.

3.2 Description of Stimuli

As mentioned earlier, the main goal of the study is to demonstrate the ability of extracting the per stimulus response of ERG with the use of high frequency stimuli, as well as investigating the effect of using the high-stimulating rate on the implicit time and amplitude of the extracted transient ERG's main components. To achieve these goals, three types of stimuli besides the conventional transient ERG stimulus of 2 Hz were designed. To deliver the stimulation sequences of a white LED light with a sweep length of 500 ms, steady state sequences, CLAD sequences and RAD sequences. The basic stimulus characteristics are listed in Table 3.1.

3.2.1 Steady State Sequences

Steady state stimuli sequences are known as isochronic sequences. As mentioned previously, steady state sequences are designed in a way that assures having equal inter-stimulus intervals between each flash stimulus in the sequence. Thus, five steady state

stimuli were created with inter-stimulus intervals equally spaced of 100, 66.67, 31.25, 20, and 14.71 ms to deliver stimulation rates of 10, 15, 32, 50 and 68 Hz respectively.

Table 3.1: Characteristics of Stimulus Sequences Used in the Study.

	Steady state		Quasi steady state			RAD	
Rate	Length (samples)	No. of stimulus	Length (samples)	No. of stimulus	NAF	Length (samples)	No. of stimulus
2 Hz	1024	1	1024	1	1.00	1024	1
10 Hz	1000	5	1020	5	0.71	131072	31
15 Hz	1064	8	1206	9	0.48	131072	31
32 Hz	1024	16	1024	16	0.38	131072	31
50 Hz	1000	25	1000	25	0.38	131072	31
68 Hz	1015	35	1008	36	0.35	131072	31

Note. Currently, the mean RAD computation is not implemented.

3.2.2 CLAD Sequences

As mentioned in section 2.6, CLAD sequences introducing a short amount of delay or advancement on the stimulus onset are called Quasi Steady State (QSS) sequences. This short variation in the sequence onset gives the ability to extract per-stimulus-evoked ERG nearly at any stimulation rate higher than 10 Hz. For the purpose of this study, the QSS sequences were generated by a CLAD sequence module. In this module, the user enters the required rate of stimulation and the program produces the proper sequence that can represent the stimulus (Delgado & Ozdamar, 2004). For this study, five jittered sequences with stimulation rates of 10, 15, 32, 50, and 68 Hz were generated.

These jittered sequences have mean inter-stimulus intervals of 100, 66.67, 31.25, 20, and 14.28 ms, respectively. Temporal distributions, rate histograms and noise amplification factors (NAF) of these sequences are displayed in Figure 3.1.All sequences were generated with a mean deconvolution gain factor or noise amplification factor below the threshold of one. For instance, as shown in Figure 3.1, the rate histogram of the

32 Hz sequence illustrates how the frequency is distributed around 32 Hz. Moreover, the mean of the noise amplification factor for 32 Hz sequence is 0.38 with a few noise amplification bands.

3.2.3 RAD Sequences

In CLAD sequences, the slight jittering introduced to the sequence is periodic. Which repeat itself every 500 ms. However, RAD stimulating sequences are designed with random inter-stimulus intervals with no repetition. This sequence is designed in a way to have a similar histogram of the periodic sequence.

In order to control the adaptation effects, the range of the random inter-stimulus intervals (ISI) of the sequence has to be limited. To design proper sequences for a study, an ISI histogram is defined. In a RAD sequence generation procedure; there is the assumption of having a sampling rate for the sequence equal to the sampling rate of the acquired signal. Therefore, the ISI random variables following the probability density function are discrete values ranging from a minimum ISI to a maximum ISI that are defined by its histogram.

Five RAD sequences with stimulation rates of 10, 15, 32, 50, and 68 Hz were created to serve the study of the high stimulation ERG. All sequences had noise amplification factors below one with few points above one. The rate histograms and the NAFs of all five RAD sequences used in the study are displayed in Figure 3.2.

3.3 Instrumentation and Recoding

3.3.1 Instrumentation

SEP-CAM, a commercial two channels acquisition system developed by Intelligent Hearing Systems, Miami FL, was used to acquire the recorded signals and deliver stimulation sequences. The acquisition system has built-in software that provides

the capability to pre-set values such as the gain and filter setting, as well as the number of sweeps. All acquired raw ERG were digitized at a sampling frequency of 2000 Hz, band-pass filtered from 1 to 300 Hz and amplified by a gain of 100,000.

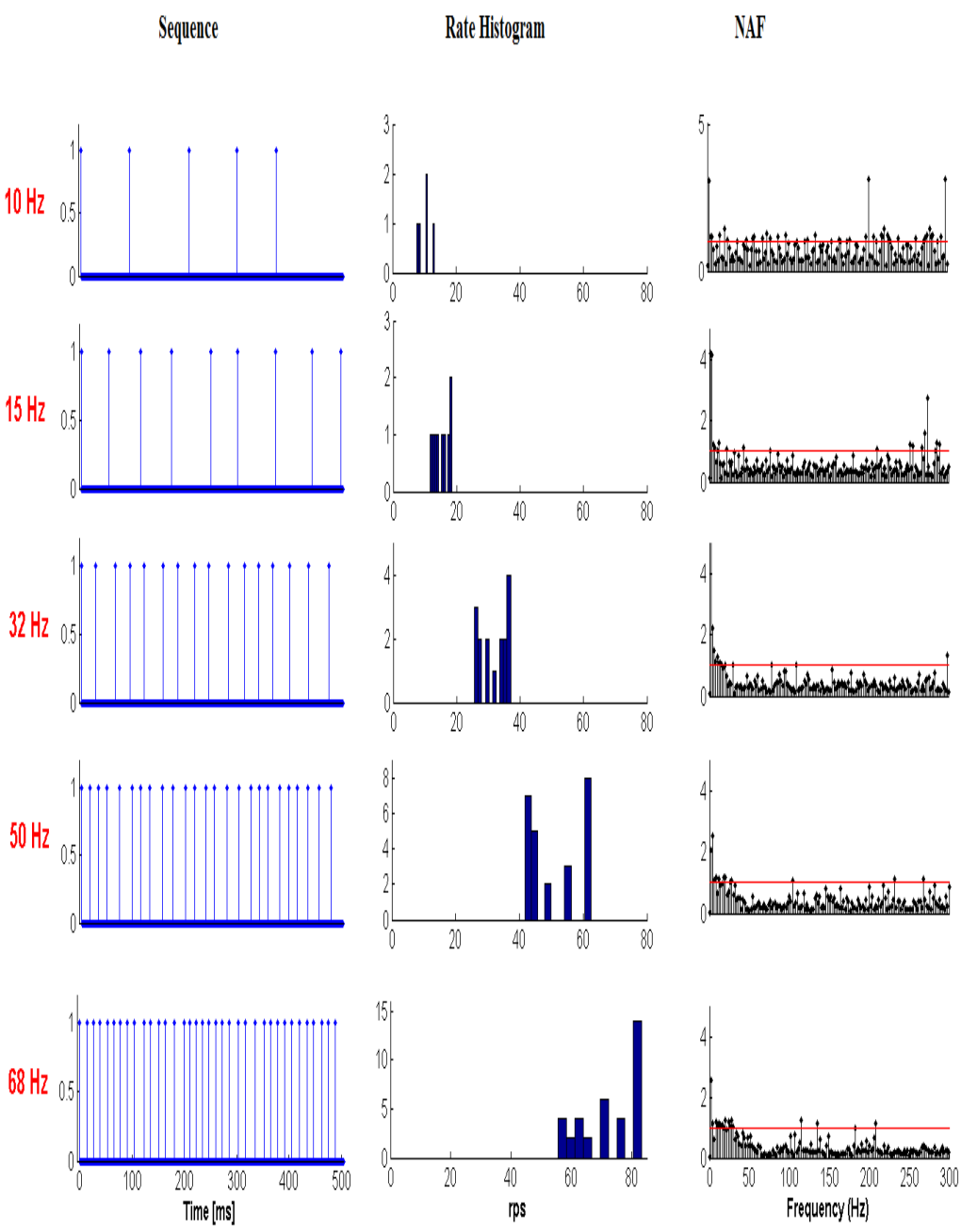

Figure 3.1: (Left column) QSS sequences with rates of 10,15,32,50 and 68 Hz showing temporal occurrence of each stimulus; (Middle column) the rate histograms and (Right column) the noise amplification factors of the same sequences.

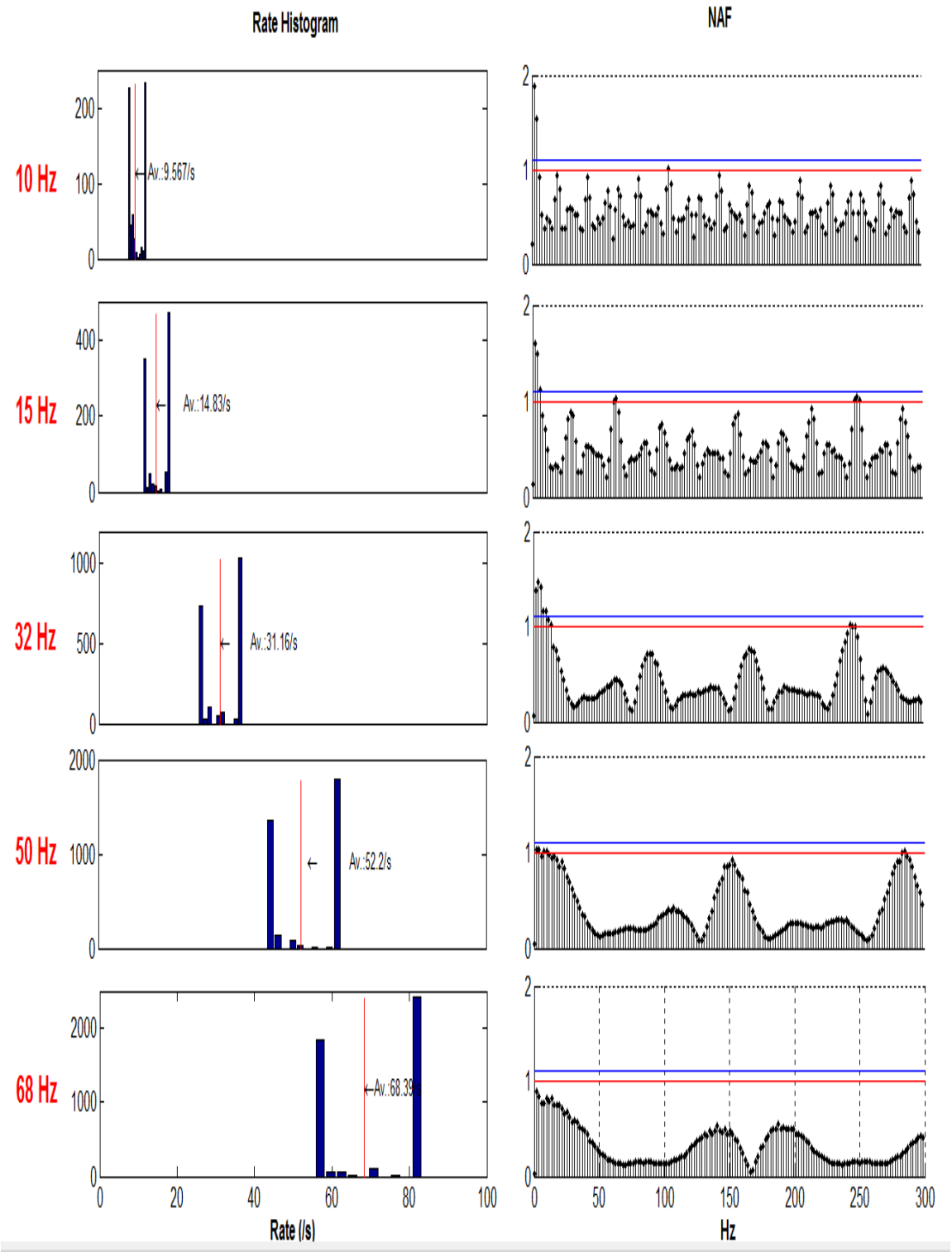

Figure 3.2: RAD sequences at rates of 10, 15, 32, 50 and 68 Hz showing (Left column), the rate histograms and (Right column), the noise amplification factors (NAF).

In this study a specially designed white LED based visual display unit (VDU) covering an angle of 33o vertical by 38o horizontal with 300 cd/m2 luminance was used. (Toft-Nielsen et al., 2011). This VDU was suitable for flicker response deconvolution since it was able to deliver 5 ms pulses of light with rise and fall times less than 200µs with stimulation strength of 1.50 cd.s.m-2 (Toft-Nielsen, 2012).

3.3.2 Subjects and Measurements Perpetration

After giving the subjects enough time to read and sign the consent forms, the recording surface was gently scraped below the eyelids with swaps in order to remove any dead skin or oil that may cause high impedance affecting the recordings. The measurement in this study was monocular, using gold skin electrodes placed on the forehead and under the eyelids. The active electrode was placed below the eyelid of the dominant eye for each subject where the reference electrode was placed on the other eye. The reference eye was then blocked by a patch (Figure 3.3). The ground electrode was placed on the forehead. All electrodes were placed with a medical grade conductive gel to enhance the conductivity. After the electrode placement, the subjects were directed to the electrically isolated dim recording chamber. The electrodes were plugged into a bio-amplifier. Then, the impedance of the placed electrodes was tested to ensure that the impedance is below 3000 ohms. The bio-amplifier is connected to the acquisition box with a fiber optic cable.

3.3.3 Data Collection

Acquiring the ERG process was done by sending the designed sequences to the acquisition system that delivers pulses, causing the visual display unit to flash based on the selected stimulus frequency. Meanwhile, the ERG responses at the selected rate were

recorded. For the study, three trials of steady state, quasi steady state, and RAD responses for all seven subjects were recorded. Three blocks were used for each mode.

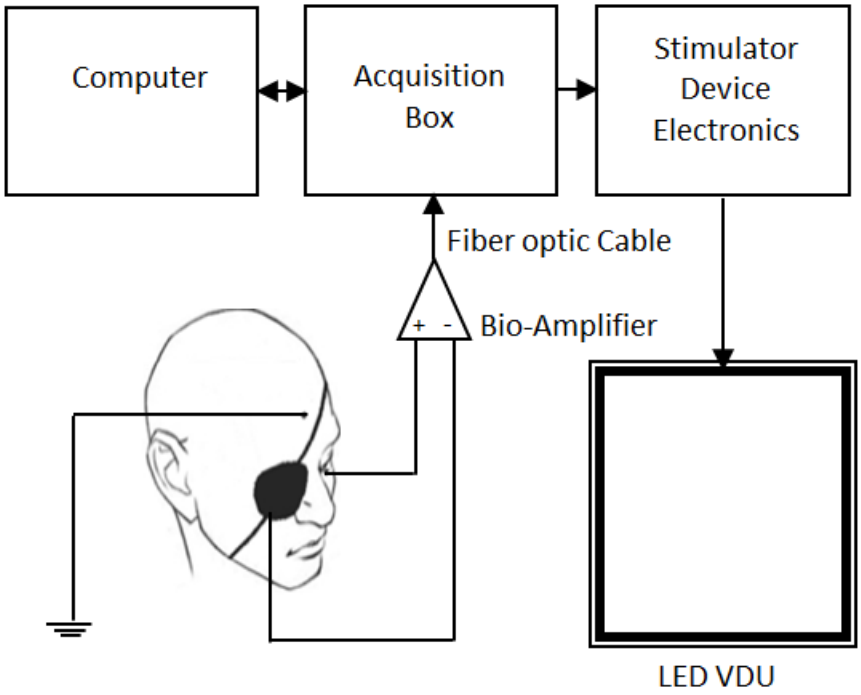

Figure 3.3: The experiment setup: the active electrode is placed under the eyelid, and the reference electrode is placed under the occluded eye. The ground electrode is placed on the forehead. The electrodes are connected to the acquisitioning box via an optical cable. The acquisitioning box is connected to a personal computer and the stimulator drive electronics. The electronic drive stimulus delivers any selected sequence to the visual display unit (VDU). The personal computer is controlled by the user to control the process of delivering the sequences and the data analysis.

3.3.3.1 Steady State

In the first block, the steady state responses were obtained for each subject at stimulation rates of 2, 10, 15, 32, 50, and 68 Hz. For each subject, three separate recordings at each rate were obtained using an isochronic steady state sequence. Each recording had 128 sweeps with a sweep length of 500 ms. Thus, 384 total sweeps were acquired for each subject at each rate. The total time for acquiring the steady state response of 2304 sweeps for each subject at all frequencies was 19.2 minutes.

3.3.3.2 Quasi Steady State

In the second session, the slightly jittered sequence (QSS) was used to record the ERG responses at the rate of 2, 10, 15, 32, 50, and 68. For each stimulation rate, three separate recordings for each subject were obtained using a quasi steady state sequence. Each recording contained 128 sweeps with a sweep length of 500 ms. Thus, 384 total sweeps were acquired for each subject at each rate. The total time for acquiring the quasi steady state response of 2304 sweeps for each subject at all frequencies was 19.2 minutes.

3.3.3.3 RAD

In the third session, the RAD sequence was loaded to the system and used to as stimulus of the ERG at the rate of 2, 10, 15, 32, 50, and 68. For each stimulation rate, three separate recordings for each subject were obtained with the RAD sequence. Each recoding contained 1 long sweep. Thus, three total sweeps were acquired for each subject at each rate. The total time for acquiring the ERG responses using RAD sequences of 54 sweeps for each subject at all frequencies was 19.2 minutes.

3.4 Signal Processing

After obtaining the raw ERG responses, all evoked potentials were processed offline using MATLAB to determine the per stimulus response for all frequencies. For each subject, we obtained the overall average of the three recordings at each rate and eliminated any noisy response that may lead to signal degradation using (MATLAB, R2012a) by adjusting the feature of artifact rejection to exclude any signal with artifacts outside of ± 30μV region. The ERG transient responses of 2 Hz were averaged for each subject and used as control to the other per-stimulus ERG transient responses extracted from QSS and RAD sequences at higher rates.

3.4.1 Steady State Responses

The raw ERG responses elicited in response to isochronic sequences of 10, 15, 32, 50, and 68 Hz were averaged to generate the real steady state responses of the ERG at each stimulation rate. By maintaining the main frequency of each stimulus and the first nine harmonics, all steady state responses were denoised. The resulting steady state responses were temporally analyzed to measure the implicit time and amplitude of the b-wave (Birch, 2006).

3.4.2 Transient ERG Responses

For each rate, all data acquired in response to the slightly jittered QSS and RAD sequences were averaged individually at each rate for each subject. These responses represent the convolved response. Thus, the transient response was extracted for each stimulation rate of 10, 15, 32, 50, and 68 using CLAD and RAD algorithms. Then all transient responses for each subject at each rate were averaged. From the deconvolved transient responses, temporal analysis was conducted to obtain the amplitude and implicit time of the a-wave and the b-wave.

3.4.3 Synthetic Steady State

Assuming steady state superposition, the deconvolved transient response was used to generate the synthetic steady state in order to validate the acquired QSS transient responses. Creating the synthetic steady state was done by shifting the deconvolved transient response by 500 ms then adding the shifted responses together as in Figure 3.4. The number of shifts is based on the number of stimulus of each sequence at each frequency. The comparison between the real steady state and synthetic steady state in time domain were done by computing the correlation coefficient. Moreover, the phase and magnitude measurements were accomplished in the frequency domain.

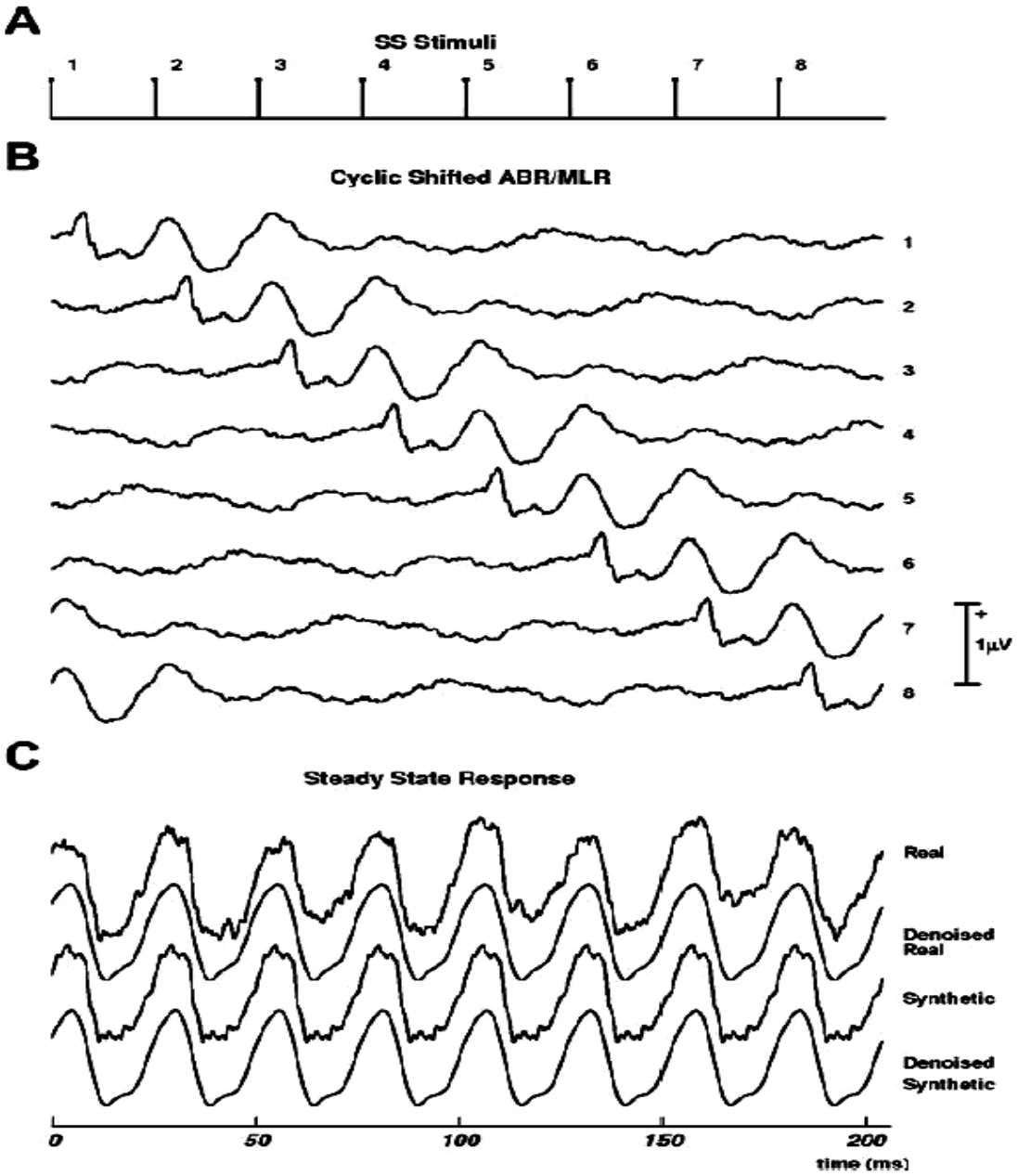

Figure 3.4: "Time domain construction of the synthetic ASSR using the low- jitter 39.1 Hz response. (A) The 39.1 isochronic stimulus sequence with each click in the sweep labeled from 1 through 8. The following eight rows in (B) correspond to the cyclic time shifted low- jitter 39.1-Hz deconvolved responses. (C) The first two rows show the separately acquired ASSR (raw) and its spectral filtered version (denoised). The bottom two rows show the summated response (synthetic) obtained by adding all the eight shifted responses shown in (B) and its filtered version (denoised synthetic)". From (Bohórquez and Ozdamar, 2008).

3.5 Statistical Analysis

The denoised acquired responses were analyzed in time domain to identify the response implicit times and amplitudes. For the deconvolved transient responses acquired using QSS and RAD sequences, the a-wave and b-wave amplitude and implicit time were quantified as defined in Marmor et al. (2009). Furthermore, the amplitude and implicit time the steady state responses were measured as in Birch, (1991). The population average, standard deviation and the statistical t-test were computed in order to study the relationship between the responses at each method for all stimulation rates.

Chapter 4

Results

In this chapter, we demonstrate the results of applying the methods and principles described earlier in chapter three to achieve the goals of this study. All recordings were recorded a sweep length of 500 ms. Since no appreciable responses were identified after 250 ms, only first 250 ms of recordings are shown in all of the following figures.

4.1 The Conventional Transient FERG

The conventional transient FERG is the evoked potential that results as a response to a stimulation sequence that has inter-stimulus interval longer than the ERG response. In another word, the ERG response settles completely before delivering the next stimulation onset. In this study, the conventional transient ERG was acquired at 2 Hz from seven subjects as shown in (Figure 4.1). The conventional transient FERG was collected to ensure the validity of having a clear and quantifiable FERG response to be used as a reference to compare with FERG responses deconvolved from higher stimulation rates. Figure 4.1 shows the 2 Hz FERG for all subjects and their overall population average. We can recognize the a-wave and b-wave. However, there is amplitude variability between the subjects. Also, at approximately 25 ms we can observe the oscillatory potentials.

4.2 Steady State Responses

For the stimulation rates higher than 10 Hz, the FERG responses start to overlap with each other resulting in steady state responses. Since the inter-stimulus intervals used in steady state sequences are periodic and equal, per stimulus FERG response cannot be deconvolved due to response matrix singularity. Thus, most of the temporal information in the FERG responses is irrecoverably lost. However, from the FERG responses, we

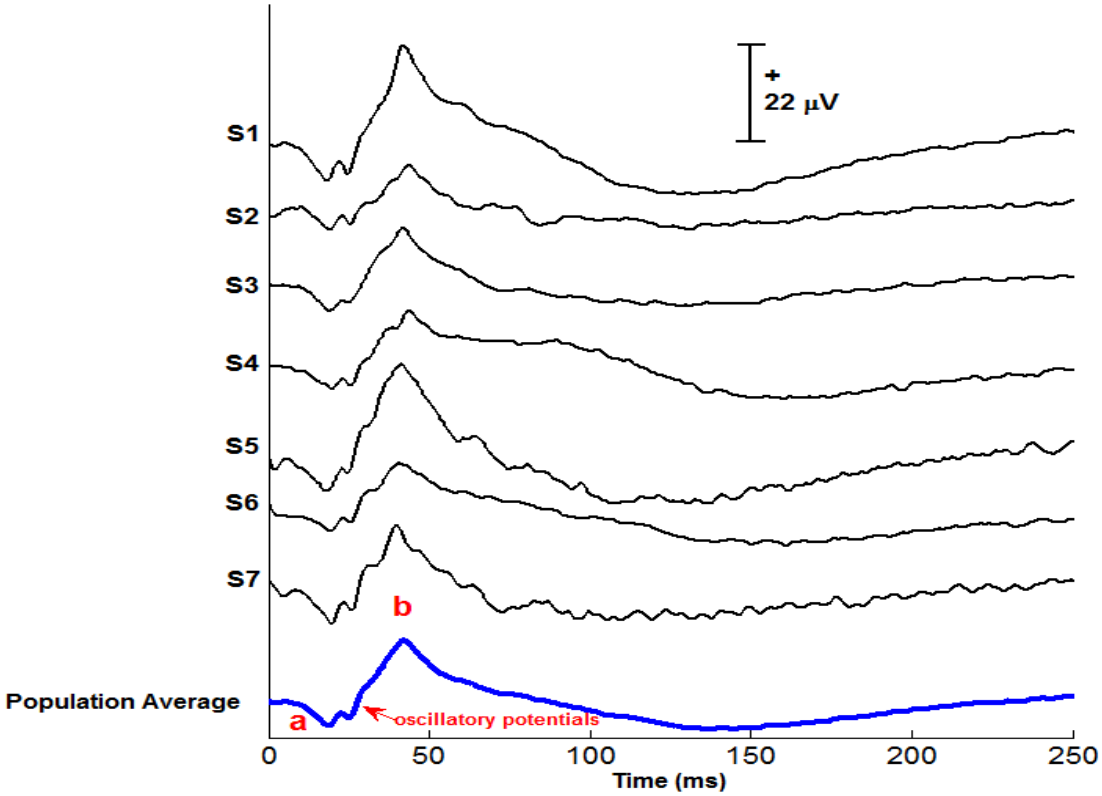

Figure 4.1: The conventional transient response of 2 Hz for each subject and the population average in blue. A-wave, b-wave and oscillatory potentials are marked on the figure.

analyzed the implicit time and amplitude of b-wave (Table 4.1) as in (Birch, 2006). The resulted responses showed clearly that the decrease of the responses amplitude and implicit time is occurring as the stimulation rate increases. The resulted population average recorded from seven subjects are shown in (Figure 4.2) below.

The waveforms amplitude and implicit time in Table 4.1 were computed using measurements obtained from seven subjects as previously described. From the temporal analysis, we can infer a little variability between the seven subjects. Also, it can be clearly seen that as the stimulation rate increases, the amplitude and implicit time of the waveforms decrease. At 10 Hz, the population average of the waveform implicit time is 39.03 with standard deviation of 1.27 and average amplitude of 13.41 with standard

Table 4.1: Steady State Amplitudes and Implicit Times of the b-Wave for Seven Subjects at for All Stimulation Rates.

Steady state	10 Hz		15 Hz		32 Hz		50 Hz		68 Hz	
	Implicit time	Amplitude	Implicit time	Amplitude	Implicit time	Amplitude	Implicit time	Amplitude	Implicit time	Amplitude
S1	39.60	14.07	39.10	7.46	30.60	4.10	30.60	5.50	27.10	0.40
S2	41.10	12.33	40.60	9.20	29.60	3.80	24.60	5.20	33.60	0.40
S3	39.60	10.58	41.10	8.70	31.10	9.30	30.10	4.20	26.10	0.70
S4	39.10	18.66	39.10	13.20	31.10	6.90	30.10	7.10	26.60	1.20
S5	38.60	19.78	38.60	12.70	29.10	4.50	29.60	4.60	24.60	0.90
S6	37.10	10.95	36.60	7.30	31.10	7.40	28.10	2.20	25.60	0.80
S7	38.10	7.52	36.10	4.86	28.60	3.20	27.60	3.20	26.60	0.30
M	39.03	13.41	38.74	9.06	30.17	5.60	28.67	4.57	27.17	0.67
SD	1.27	4.44	1.86	3.00	1.06	2.28	2.11	1.60	2.95	0.33

Note. Averages and standard deviations are listed as shown.

deviation of 4.44. At 15 Hz, the population average of the waveform implicit time is 38.74 with standard deviation of 1.86 and average amplitude of 9.06 with standard deviation of 3. At 32 Hz, the population average of the waveform implicit time is 30.17 with standard deviation of 1.06 and average amplitude of 5.6 with standard deviation of 2.28. At 50 Hz, the population average of the waveform implicit time is 28.67 with standard deviation of 2.11 and average amplitude of 4.57 with standard deviation of 1.6. At 68 Hz, the population average of the waveform implicit time is 27.17 with standard deviation of 2.95 and average amplitude of 0.67 with standard deviation of 0.33.

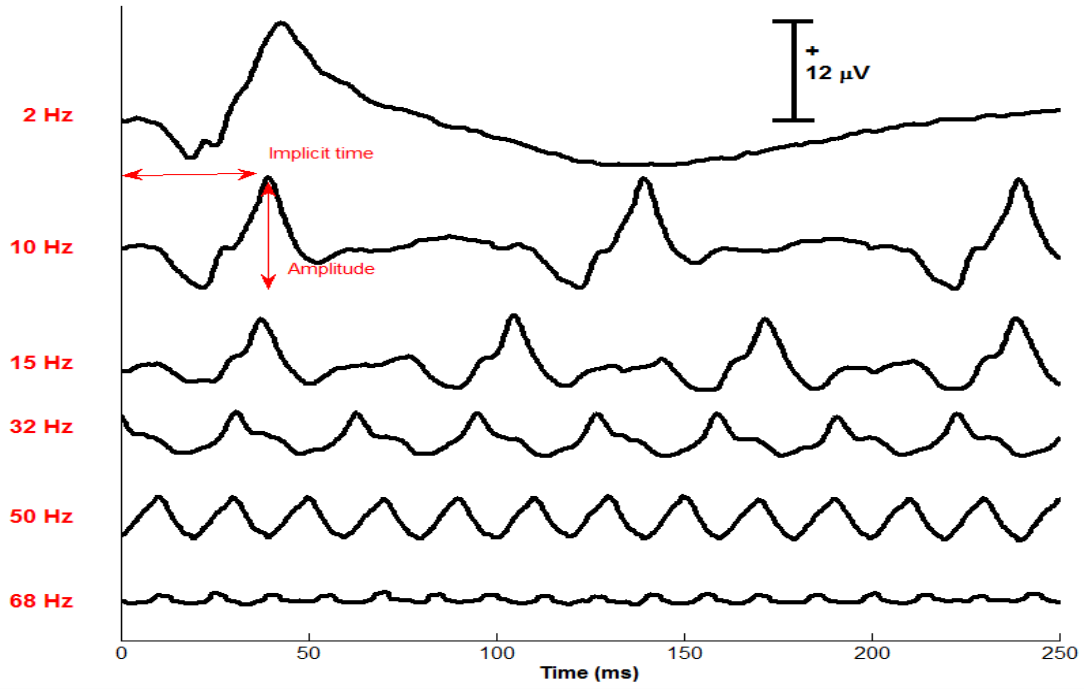

Figure 4.2: The population averages of steady state responses for seven subjects at 2, 10,15,32,50, and 68 Hz. The temporal analysis of b-wave was done by computing the b-wave amplitude and implicit time as shown.

4.3 Quasi Steady State Responses

By using the slightly jittered quasi steady state (QSS) sequences explained in 3.2.2, CLAD was successfully able to extract the per stimulus transient responses at the used high rate stimulation of 10, 15, 32, 50 and 68 with clear and quantifiable a-wave and

b-wave. Averaged deconvolved waveform components are clearly visible and consistent in both implicit time and amplitude from seven subjects with total number of 13440 sweeps with 500 ms for each sweep. Moreover, it was noticeable that as the stimulation rate increases, the implicit time and wave amplitude start to change. The resulting averaged responses at each rate for each subject and the overall population averages are shown in (Figure 4.3, 4.4, 4.5, 4.6, 4.7, 4.8) below.

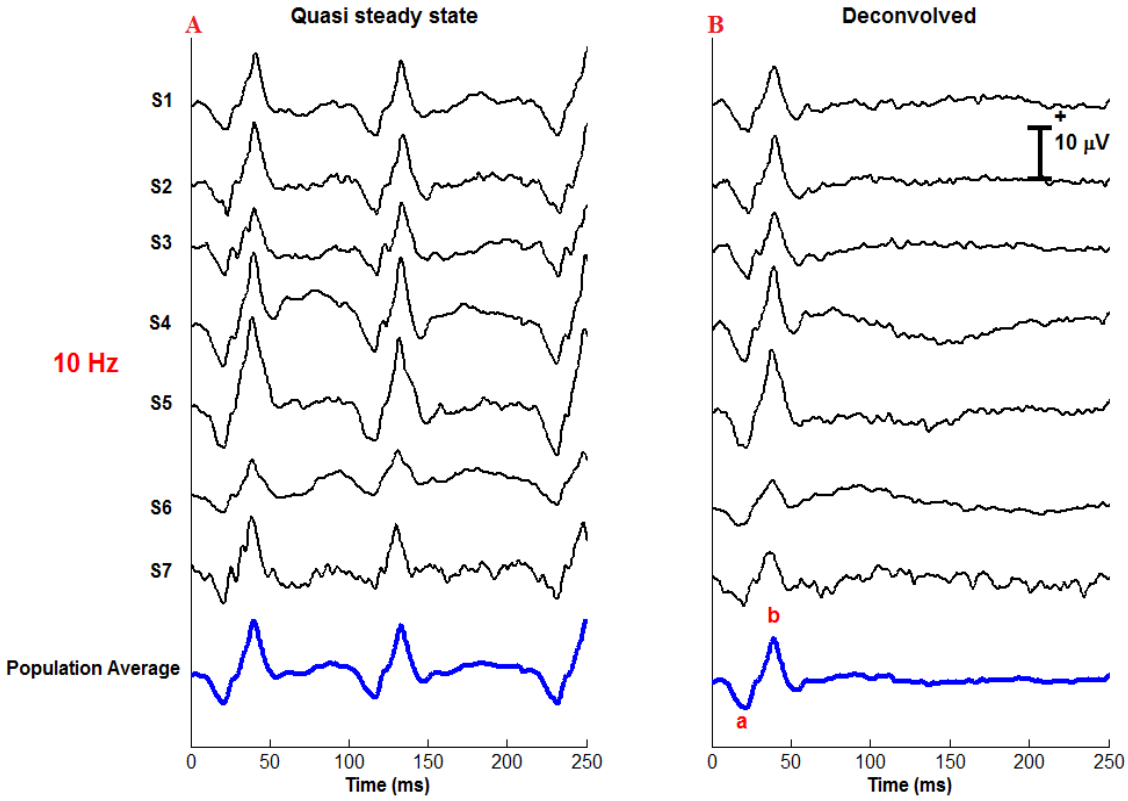

Figure 4.3: (A) The convoluted QSS response obtained at 10 Hz from seven subjects and (B) the corresponding deconvolved transient FERGs. The population averages are shown in blue in the bottom. (a-wave and b-wave) are marked.

The temporal analysis of the main components of the deconvolved FERG is illustrated in Table 4.2. The measurement of amplitude and implicit time was measured as described in Marmor et al. (2009).

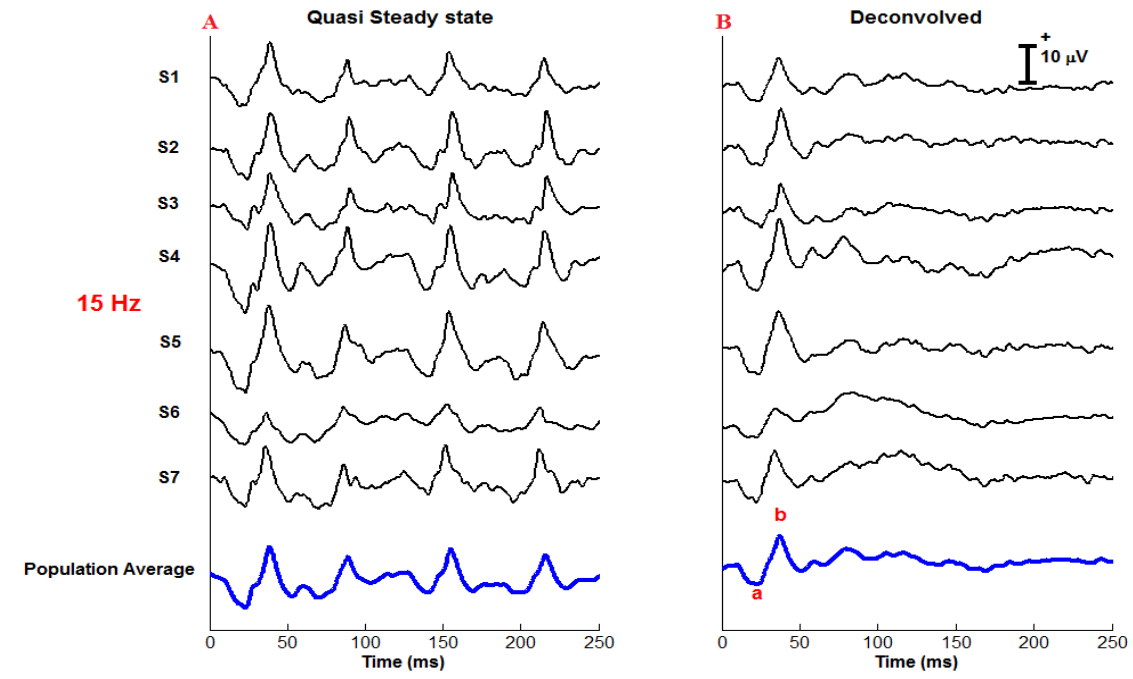

Figure 4.4: (A) The convoluted QSS response obtained at 15 Hz from seven subjects and (B) the corresponding deconvolved transient FERGs. The population averages are shown in blue in the bottom. (a-wave and b-wave) are marked.

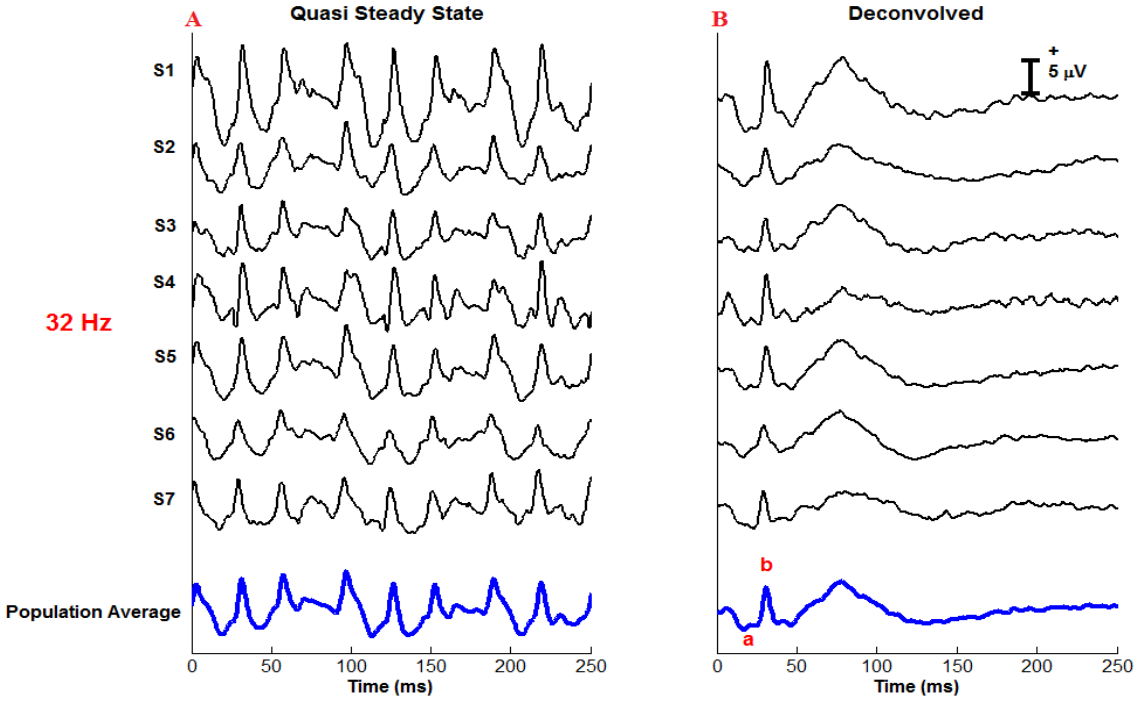

Figure 4.5: (A) The convoluted QSS response obtained at 32 Hz from seven subjects and (B) the corresponding deconvolved transient FERGs. The population averages are shown in blue in the bottom. (a-wave and b-wave) are marked.

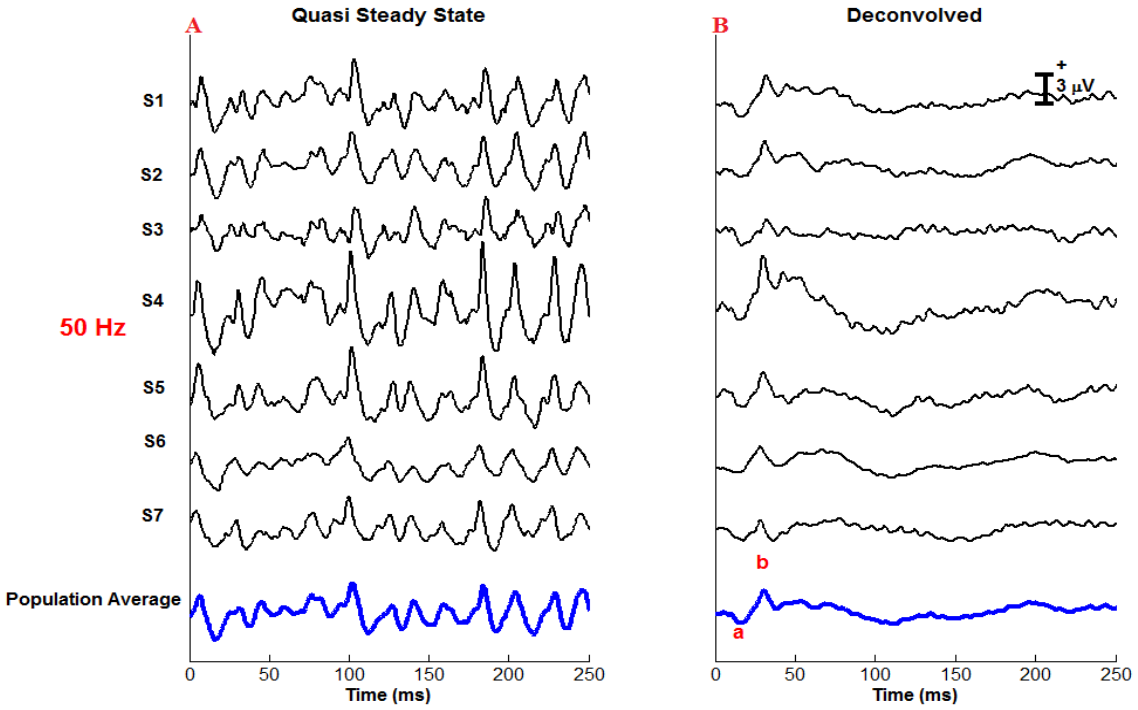

Figure 4.6: (A) The convoluted QSS response obtained at 50 Hz from seven subjects and (B) the corresponding deconvolved transient FERGs. The population averages are shown in blue in the bottom. (a-wave and b-wave) are marked.

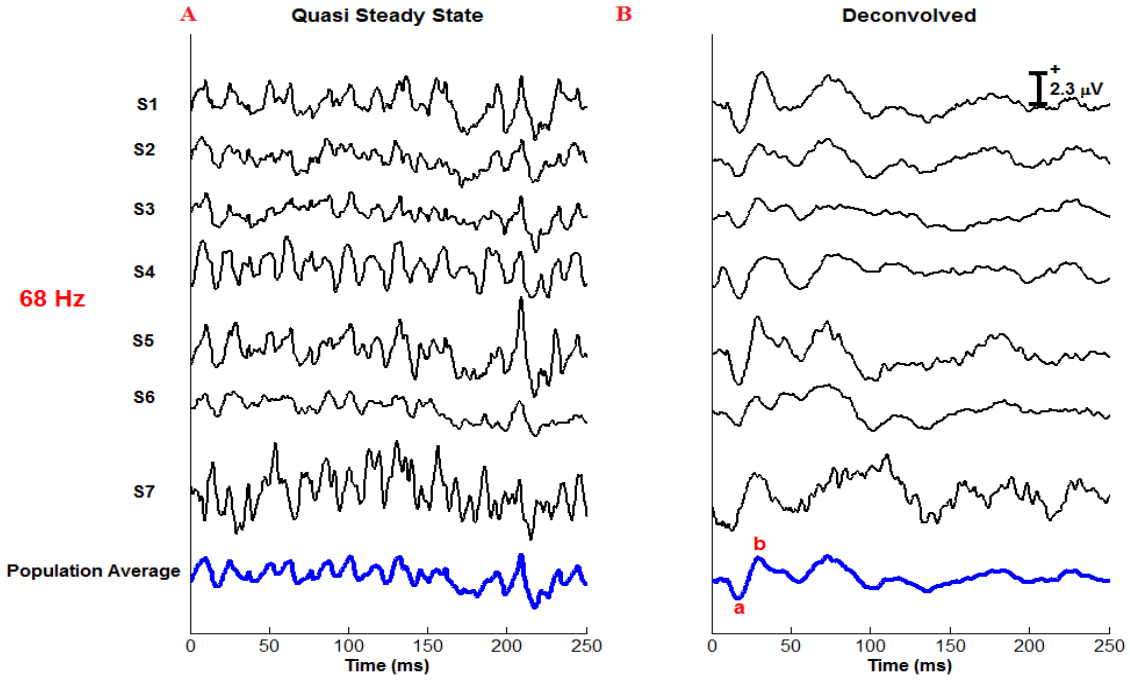

Figure 4.7: (A) The convoluted QSS response obtained at 68 Hz from seven subjects and (B) the corresponding deconvolved transient FERGs. The population averages are shown in blue in the bottom. (a-wave and b-wave) are marked.

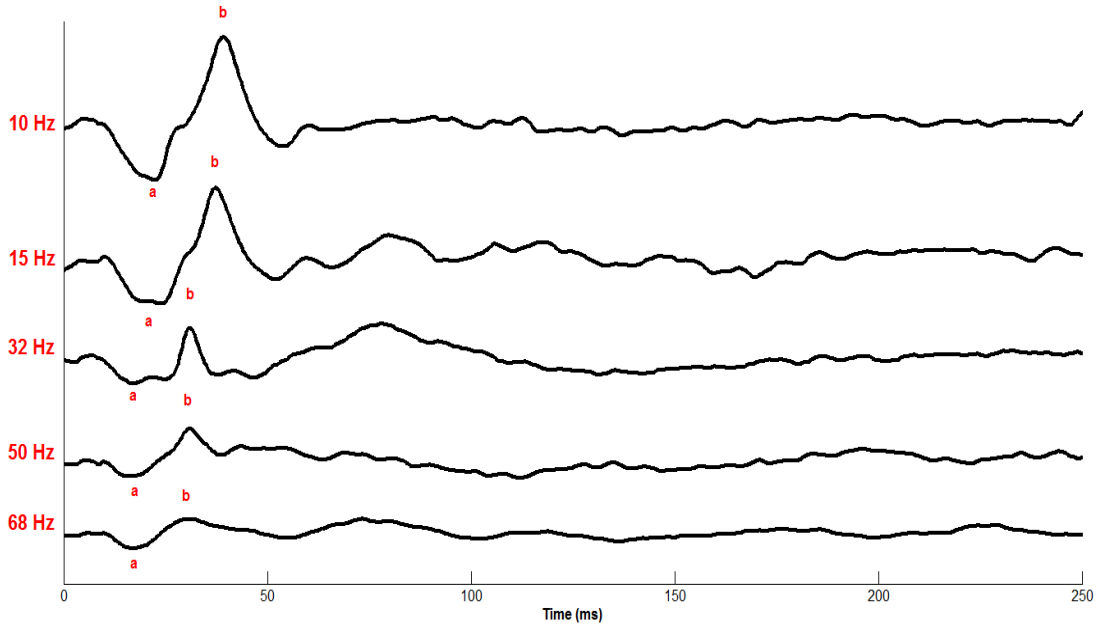

Figure 4.8: The population averages of the deconvolved transient FERG at 10, 15, 32, 50 and 68 Hz. FERG main components (a-wave and b-wave) are marked.

Table 4.2: Amplitudes and Implicit Times of the Major FERG Components (a-Wave and b-Wave) at Different Rates

Rate (Hz)	Amplitude (μV)		Implicit time (ms)	
	a-wave	b-wave	a-wave	b-wave
2	-5.61 (2.13)	18.12 (7.66)	18.81 (0.76)	41.39 (1.12)
10	-4.96 (1.04)	12.98 (3.55)	21.17 (2.19)	38.53 (1.86)
15	-3.59 (1.17)	10.53 (2.95)	21.89 (1.82)	36.31 (1.60)
32	-2.25 (1.04)	5.14 (1.62)	18.81 (2.63)	30.53 (0.89)
50	-1.16 (0.48)	4.38 (1.80)	15.88 (1.32)	30.10 (1.43)
68	-1.48 (0.76)	3.20 (2.38)	15.44 (2.19)	30.10 (2.38)

Note. Average values and standard deviations (in parentheses) of the population are shown.

At 2 Hz, the population average of a-wave amplitude is -5.61 with standard deviation of 2.13 and average implicit time of 18.81 with standard deviation of 0.76. For the b-wave, the population average waveform amplitude is 18.12 with standard deviation of 7.66 and average implicit time of 41.39 with standard deviation of 1.12. At 10 Hz, the population average of a-wave amplitude is -4.96 with standard deviation of 1.04 and average implicit time of 21.17 with standard deviation of 2.19. For the b-wave, the population average waveform amplitude is 12.98 with standard deviation of 3.55 and average implicit time of 38.53 with standard deviation of 1.86. At 15 Hz, the population average of a-wave amplitude is -3.59 with standard deviation of 1.17 and average implicit time of 21.89 with standard deviation of 1.82. For the b-wave, the population average waveform amplitude is 10.53 with standard deviation of 2.59 and average implicit time of 36.31 with standard deviation of 1.60.

At 32 Hz, the population average of a-wave amplitude is –2.25 with standard deviation of 1.04 and average implicit time of 18.81 with standard deviation of 2.63. For the b-wave, the population average waveform amplitude is 5.14 with standard deviation of 1.62 and average implicit time of 30.53 with standard deviation of 0.89. At 50 Hz, the population average of a-wave amplitude is -1.16 with standard deviation of 0.48 and average implicit time of 15.88 with standard deviation of 1.32. For the b-wave, the population average waveform amplitude is 4.38 with standard deviation of 1.80 and average implicit time of 30.10 with standard deviation of 1.43. At 68 Hz, the population average of a-wave amplitude is -1.48 with standard deviation of 0.76 and average implicit time of 15.44 with standard deviation of 2.19. For the b-wave, the population average

waveform amplitude is 3.20 with standard deviation of 2.38 and average implicit time of 30.10 with standard deviation of 2.38.

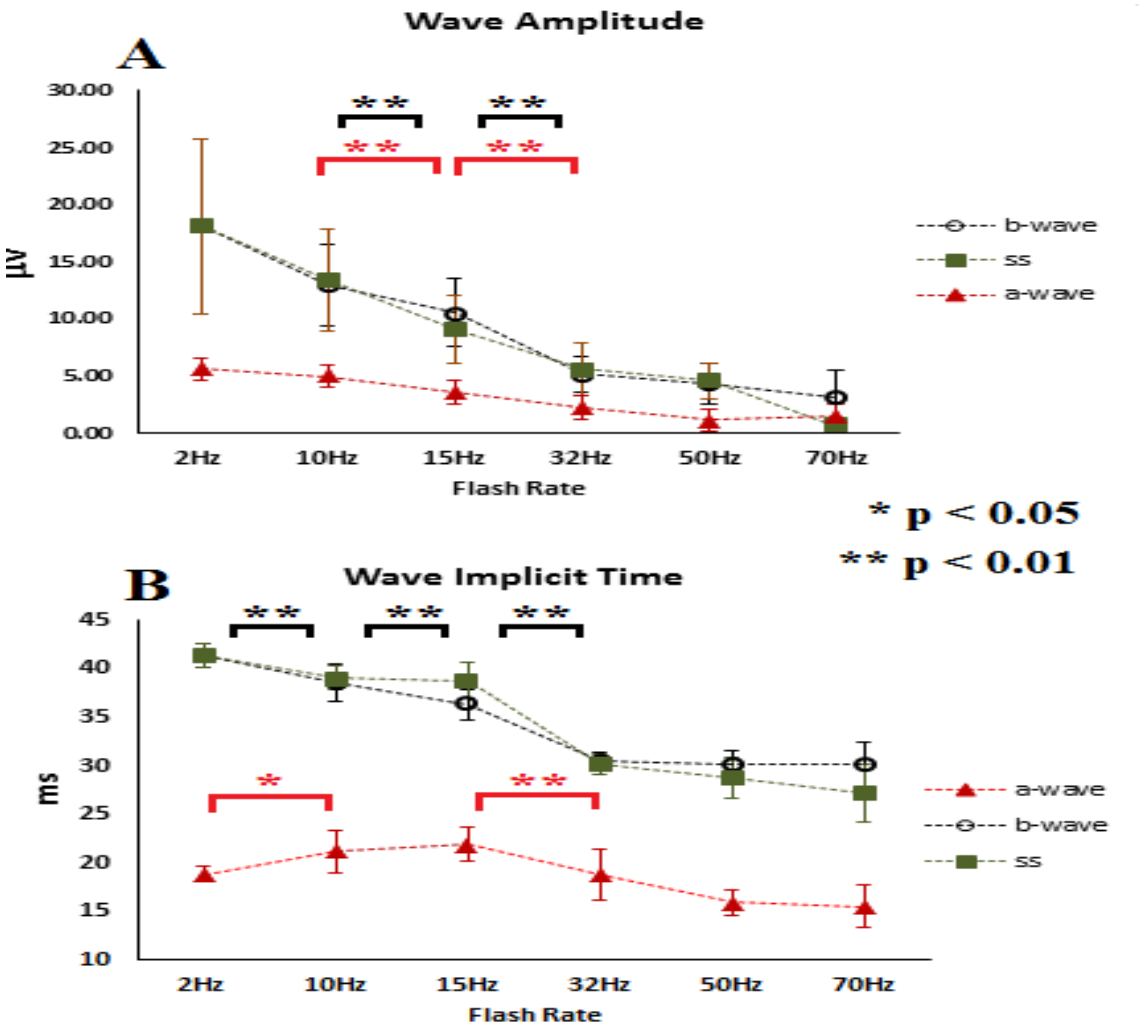

Figure 4.9: Statistical analysis of a-wave, b-wave and real SS responses acquired from the QSS sequences. (A) The amplitude of the waveforms components in microvolt. (B) The implicit time of the waveform components in millisecond. (*) shows significance of comparisons as indicators.

4.4 RAD Responses

By using long sequences with randomly jittered inter-stimulus intervals, explained in 3.3.3, RAD was successfully able to obtain the per stimulus transient responses at the used high rate stimulation of 10, 15, 32, 50 and 68 with clear and quantifiable a-wave and b-wave as CLAD (Table 4.2). Averaged deconvolved waveform components are clearly

visible and consistent in both implicit time and amplitude from seven subjects with total number of 105 sweeps. Moreover, it was noticeable that as the stimulation rate increases, the implicit time and wave amplitude start to change. The resulting averaged responses at each rate for each subject and the overall population averages are shown in Figure (4.10, 4.11, 4.12.4.13, 4.14, 4.15) below.

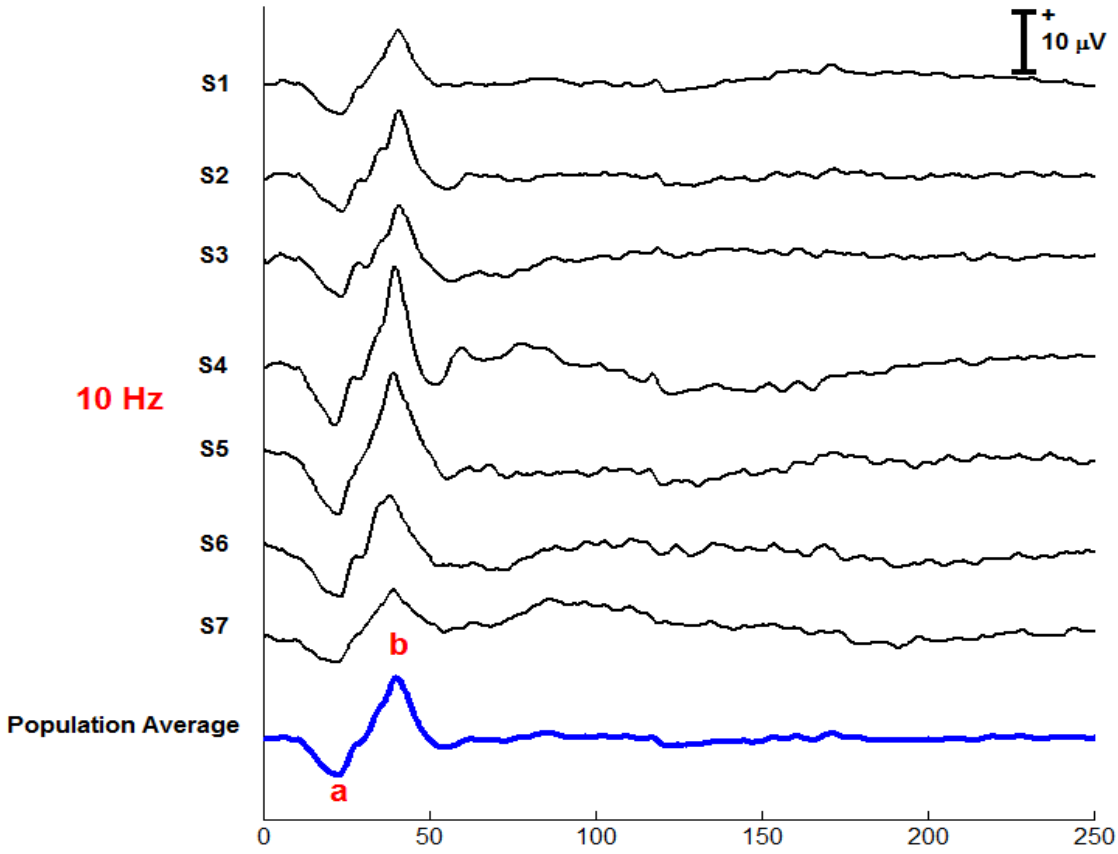

Figure 4.10: The deconvolved FERG resulting from 10 Hz non-periodic RAD stimulation sequence. The main FERG components are marked on the population average (blue trace) shown at the bottom.

The temporal analysis of the main components of the deconvolved FERG is illustrated in Table 4.3. The measurement of amplitude and implicit time were computed as described in Marmor et al. (2009).

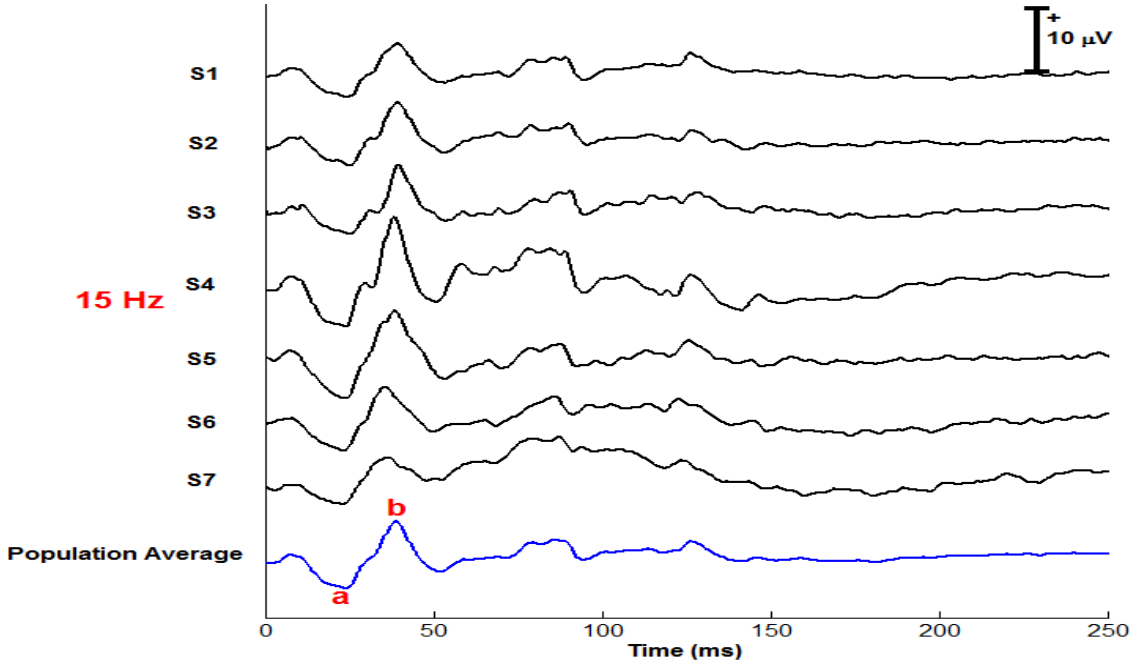

Figure 4.11: The deconvolved FERG resulting from 15 Hz non-periodic RAD stimulation sequence. The main FERG components are marked on the population average (blue trace) shown at the bottom.

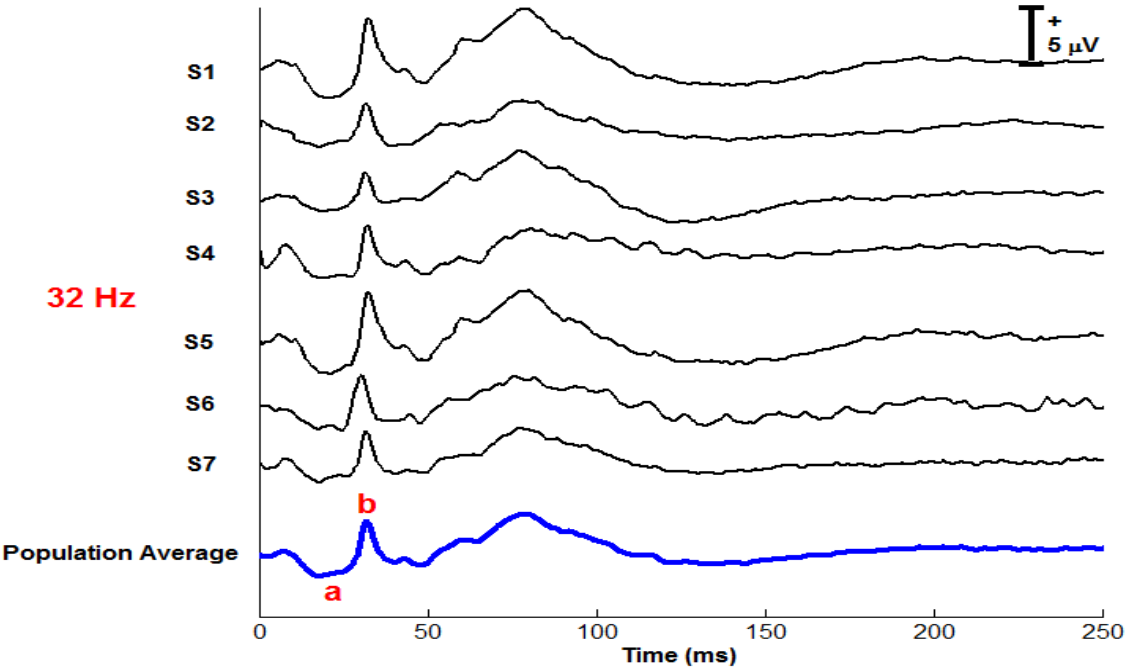

Figure 4.12: The deconvolved FERG resulting from 32 Hz non-periodic RAD stimulation sequence. The main FERG components are marked on the population average (blue trace) shown at the bottom.

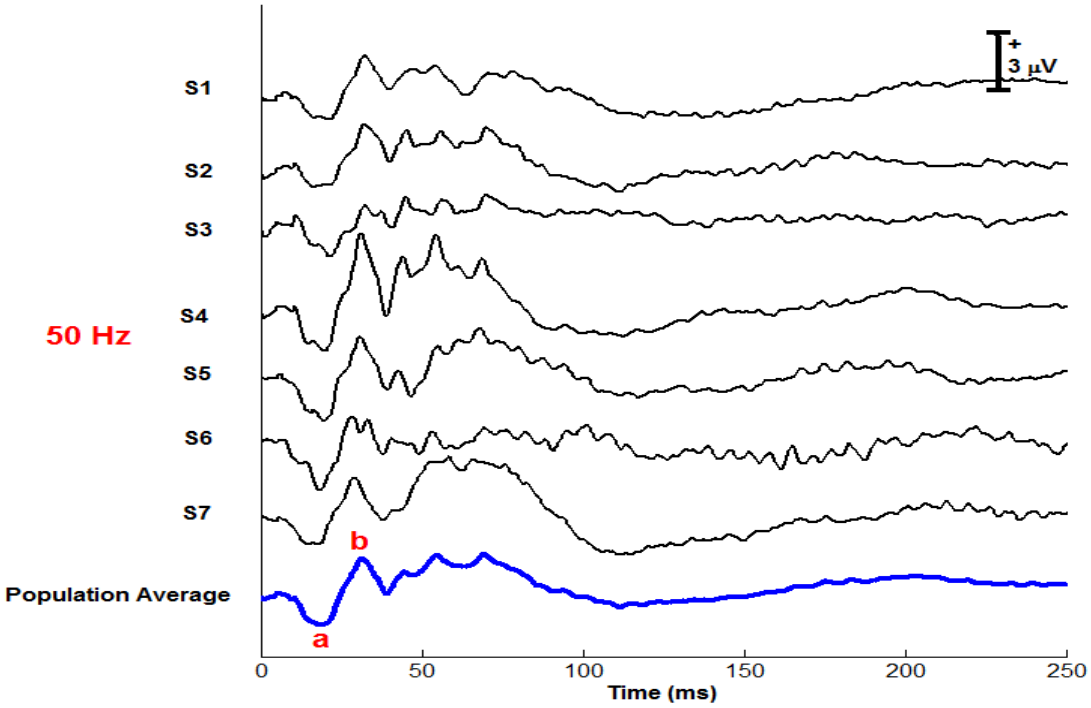

Figure 4.13: The deconvolved FERG resulting from 50 Hz non-periodic RAD stimulation sequence. The main FERG components are marked on the population average (blue trace) shown at the bottom.

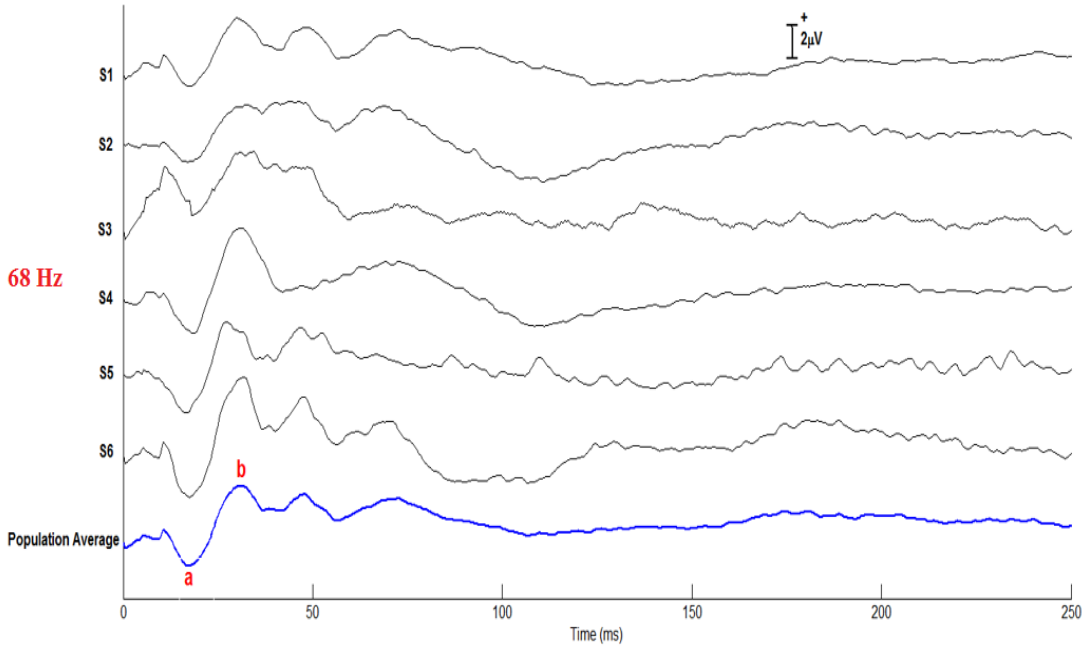

Figure 4.14: The deconvolved FERG resulting from 68 Hz non-periodic RAD stimulation sequence. The main FERG components are marked on the population average (blue trace) shown at the bottom.

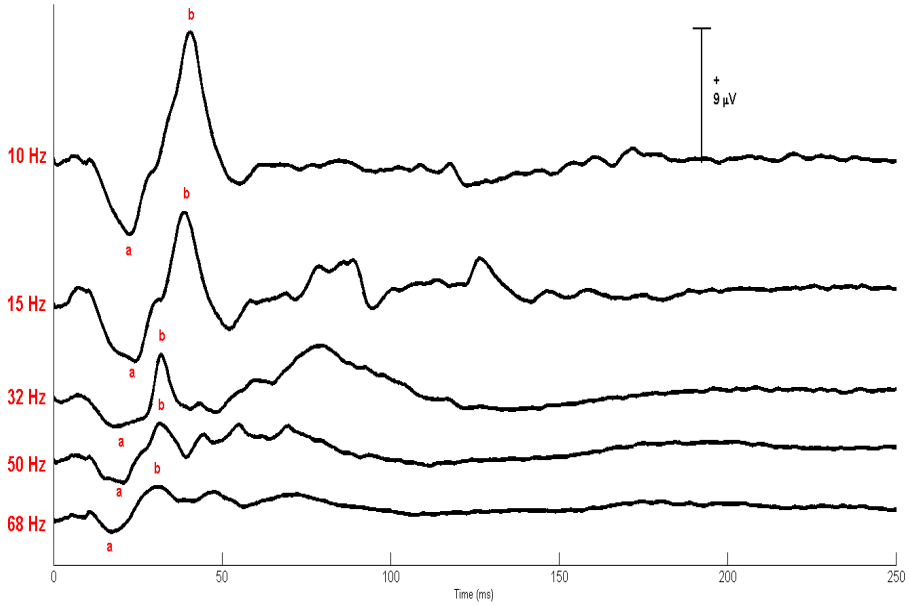

Figure 4.15: The population averages of the deconvolved transient FERG at 10, 15, 32, 50 and 68 Hz.

Table 4.3: Amplitudes and Implicit Times of the Major FERG Components (a-Wave and b-Wave) Acquired Using RAD Sequences

Rate (Hz)	Amplitude (µV)		Implicit time (ms)	
	a-wave	b-wave	a-wave	b-wave
2	-5.61 (2.13)	18.12 (7.66)	18.81 (0.76)	41.39 (1.22)
10	-5.22 (1.75)	13.38 (4.56)	22.36 (1.35)	39.86 (1.38)
15	-3.67 (1.31)	10.34 (3.13)	23.64 (0.80)	37.43 (2.73)
32	-1.91 (0.70)	4.85 (1.22)	20.67 (2.46)	31.58 (0.86)
50	-1.58 (0.78)	4.16 (1.42)	18.14 (1.14)	30.79 (1.50)
68	-1.54 (0.82)	3.24 (1.23)	15.35 (2.38)	29.35 (1.44)

Note. Average values and standard deviation (in parentheses) of the population are shown.

At 2 Hz, the population average of a-wave amplitude is -4.77 with standard deviation of 3.83 and average implicit time of 18.81 with standard deviation of 0.76. For the b-wave, the population average waveform amplitude is 18.12 with standard deviation of 7.66 and average implicit time of 41.39 with standard deviation of 1.22. At 10 Hz, the population average of a-wave amplitude is -5.22 with standard deviation of 1.75 and average implicit time of 22.36 with standard deviation of 1.35. For the b-wave, the population average waveform amplitude is 13.38 with standard deviation of 4.56 and average implicit time of 39.86 with standard deviation of 1.38. At 15 Hz, the population average of a-wave amplitude is -3.67 with standard deviation of 1.31 and average implicit time of 23.64 with standard deviation of 0.80. For the b-wave, the population average waveform amplitude is 10.34 with standard deviation of 3.13 and average implicit time of 37.34 with standard deviation of 2.73.

At 32 Hz, the population average of a-wave amplitude is –1.91 with standard deviation of 0.70 and average implicit time of 20.67 with standard deviation of 2.46. For the b-wave, the population average waveform amplitude is 4.85 with standard deviation of 1.22 and average implicit time of 31.58 with standard deviation of 0.86. At 50 Hz, the population average of a-wave amplitude is -1.58 with standard deviation of 0.78 and average implicit time of 18.14with standard deviation of 1.14. For the b-wave, the population average waveform amplitude is 4.16 with standard deviation of 1.42 and average implicit time of 30.79 with standard deviation of 1.50. At 68 Hz, the population average of a-wave amplitude is -1.02 with standard deviation of 0.47 and average implicit time of 17.42 with standard deviation of 0.49. For the b-wave, the population average

waveform amplitude is 3.27 with standard deviation of 0.98 and average implicit time of 30.42 with standard deviation of 2.25.

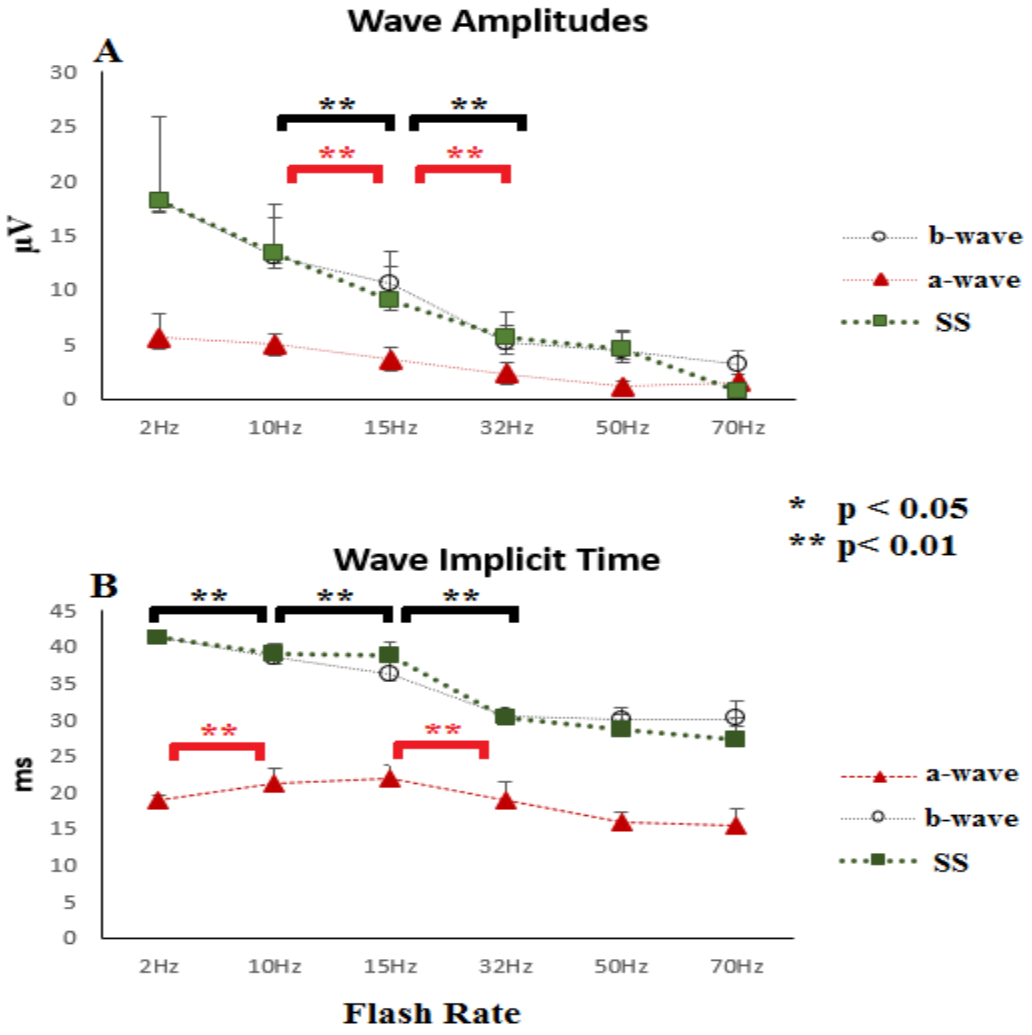

Figure 4.16: Statistical analysis of a-wave, b-wave and real SS responses acquired using the RAD sequences. (A) The amplitude of the waveforms components in microvolt. (B) The implicit time of the waveform components in millisecond.

The statistical analysis of the deconvolved FERG acquired from QSS and RAD sequences showed that, as the stimulation rate increased, the a-wave and b-wave amplitudes decreased significantly between the 10 and 15 Hz and 15 and 32 Hz. Furthermore, the implicit time of a-wave increased between 2 and 10 Hz and decreased

between 15 and 32 Hz. Moreover, b-wave decreased significantly as the stimulation rate increased up to 32 Hz as shown in Figures (4.9, 4.16).

Moreover, in comparison between FERG responses deconvolved by using CLAD and RAD deconvolution methods, the deconvolved responses showed high similarity between RAD and CLAD at stimulation rates of 10, 15 and 32 Hz. However, there are slight differences between CLAD and RAD FERG deconvolved responses acquired at 50 and 68 Hz (see Figure 4.17).

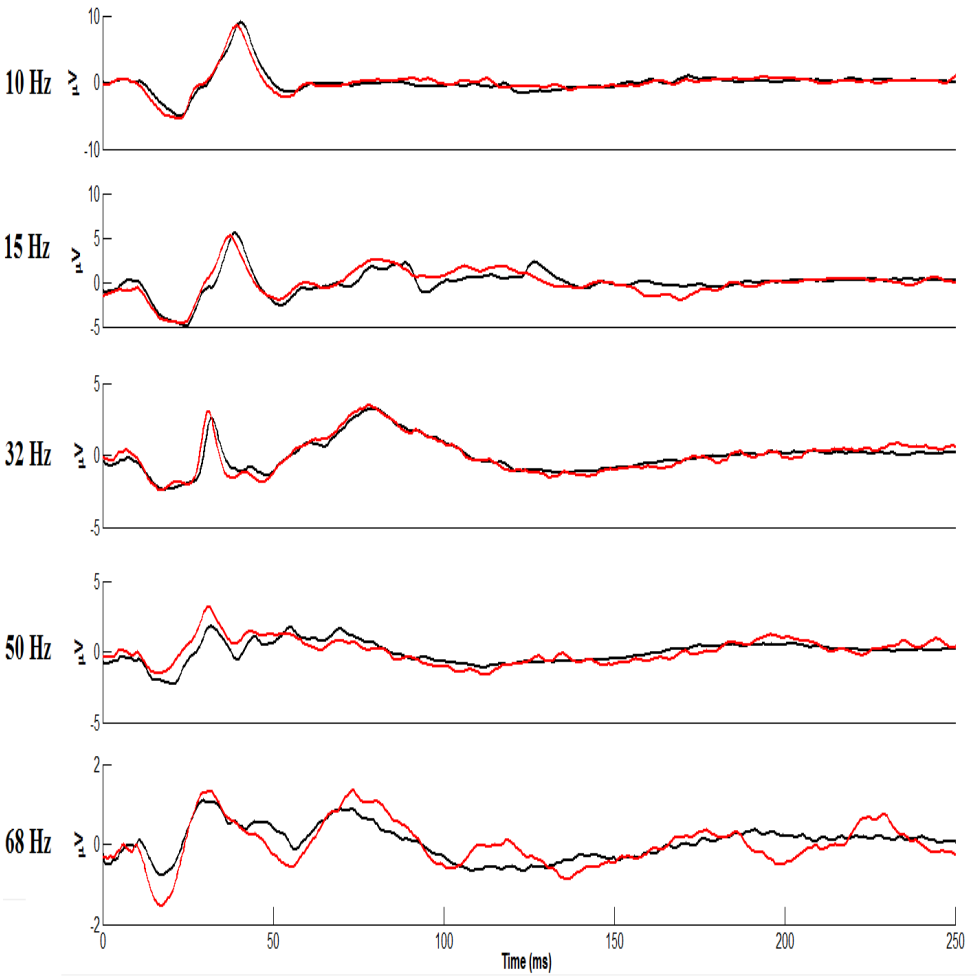

Figure 4.17: Comparison between the population averages at 10,15,32,50 and 68 Hz of FERG responses acquired in response to QSS sequences (red) and RAD sequences (black).

4.5 Synthetic Steady State Responses

The synthetic steady state responses were constructed using the transient deconvolved responses acquired by using both quasi steady state and RAD stimuli in order to validate the reliability of the deconvolved transient responses (Figure 4.18 and Figure 4.20). Time domain comparison was conducted by computing the correlation coefficient between the real steady state and the constructed synthetic steady state as shown in Table 4.3 and Table 4.4. Moreover, magnitude and phase analysis of the frequency domain was accomplished to see the differences. Phasors were used to illustrate the phase and magnitude differences between the synthetic and real steady state as shown in (Figure 4.19) for quasi steady state and in (Figure 4.20) for RAD at 2, 10, 15, 32, 50 and 68 Hz.

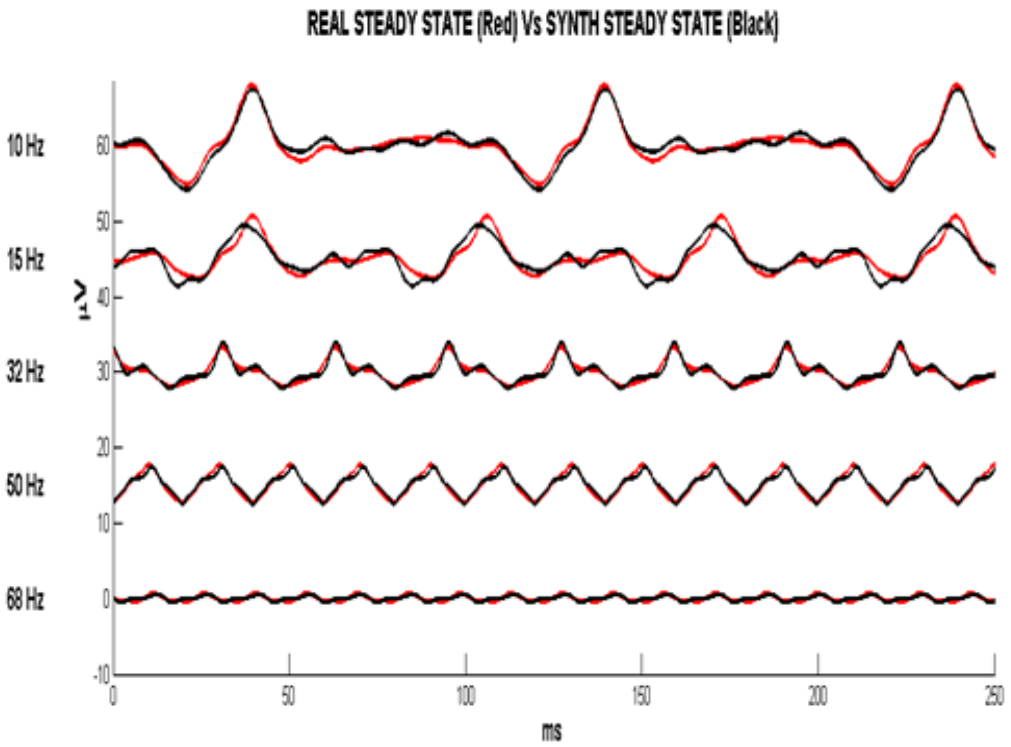

Figure 4.18: Comparisons between real steady state (Red) and the synthetic steady state (Black) constructed using the deconvolved FERG in response to quasi steady state sequence at 10, 15, 32, 50 and 68 Hz.

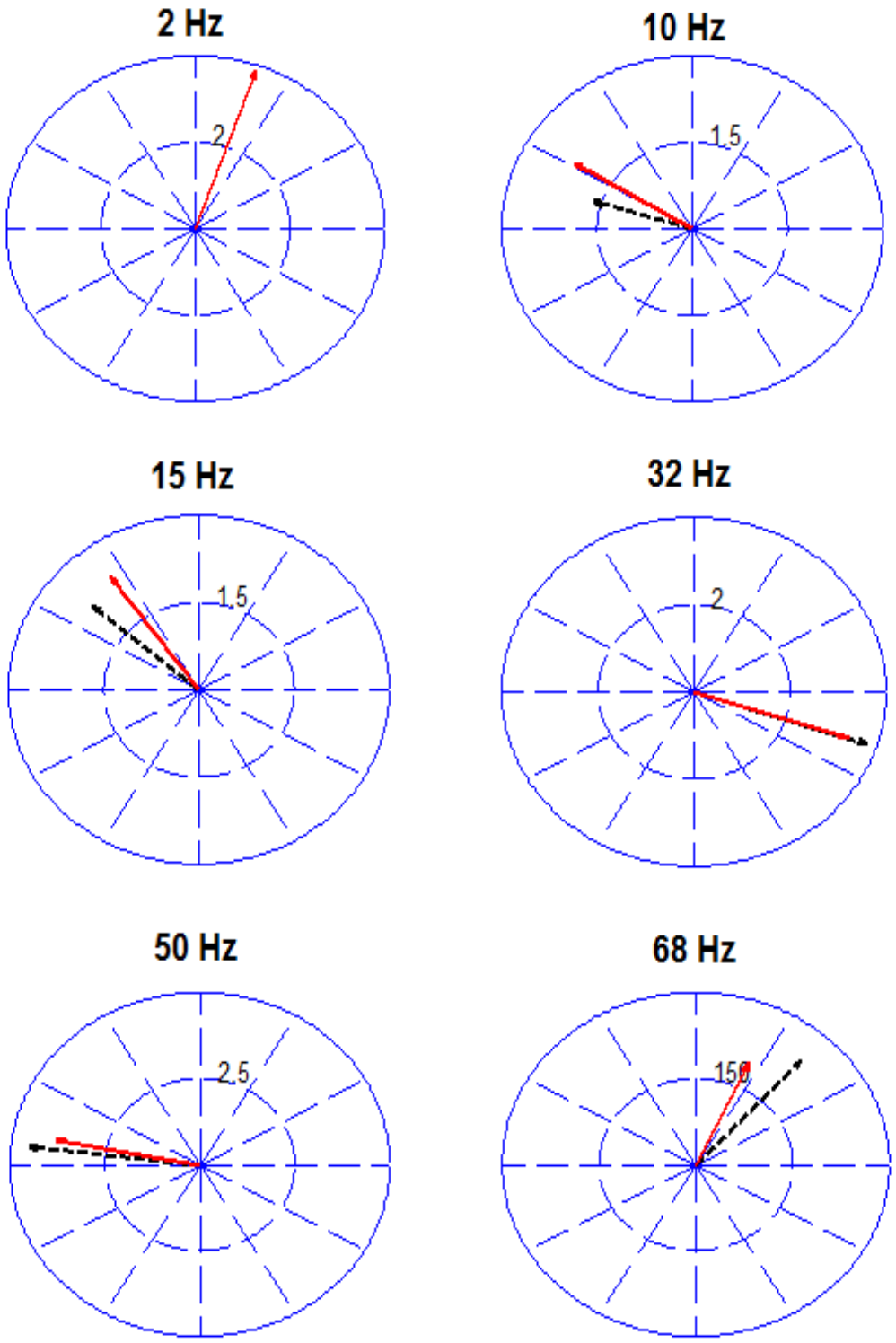

Figure 4.19: Phasor of the fundamental frequency showing the comparison of magnitudes and phases between the real steady state (black-dotted arrows) and synthetic steady state response (red arrows) delivered with using QSS sequences.

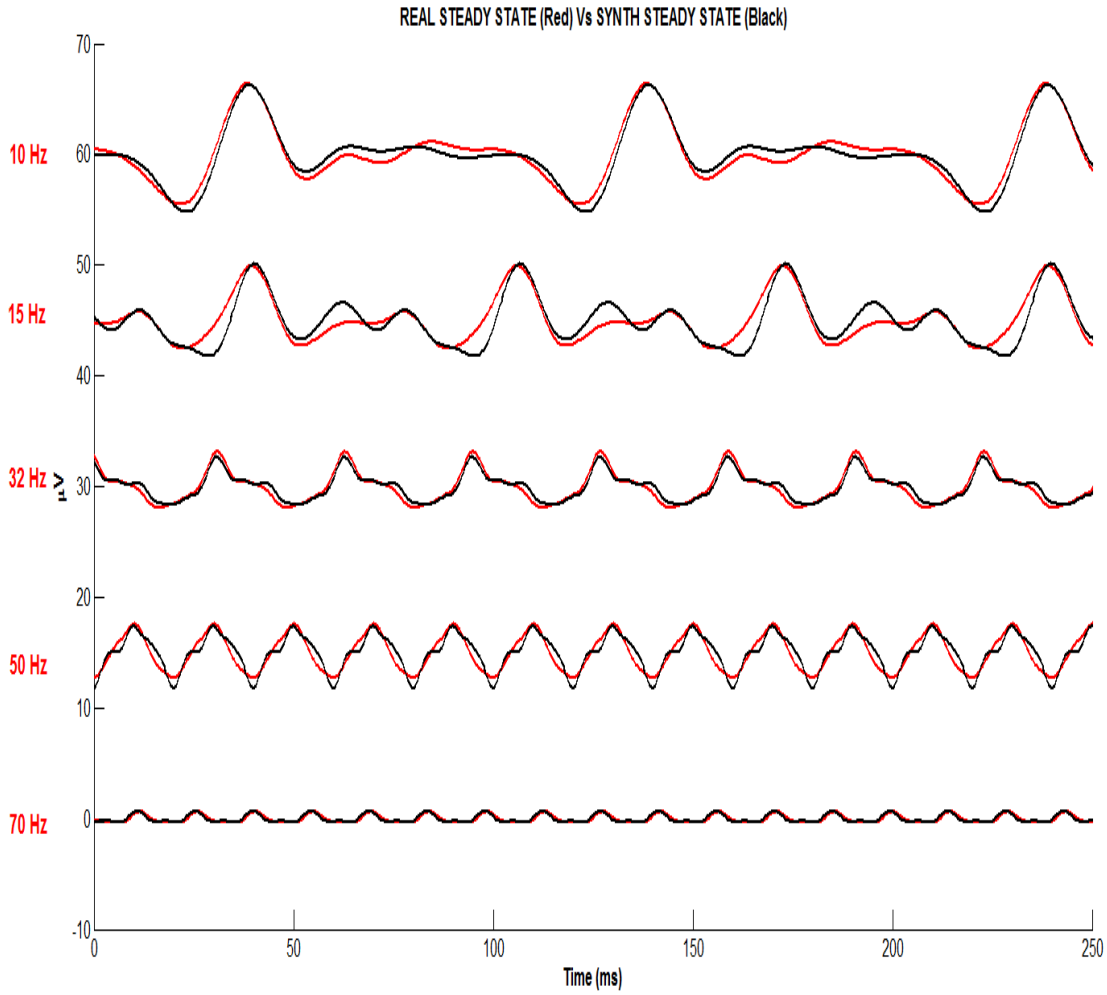

Figure 4.20: Comparison between real steady state (Red) and the synthetic steady state (black) constructed using the deconvolved FERG in response to RAD sequences at 10, 15, 32, 50 and 68 Hz.

Table 4.4: Correlation Coefficient Between Real Steady State and Synthetic Steady State

Rate (Hz)	Mean rate (Hz)	Correlation coefficient
2	1.95	N/A
10	10.00	0.97
15	15.03	0.91
32	31.25	0.95
50	50.00	0.97
68	68.98	0.82

4.5.1 Synthetic Steady State From QSS Responses

The temporal analysis using correlation coefficient between the real and synthetic steady state responses constructed from QSS sequences (Figure 4.18) showed high similarity at 10, 15, 32, and 50 Hz with lower percentage of correlation at 68 Hz for synthetic steady state responses constructed from QSS sequences as illustrated Table 4.4. In addition, frequency domain analysis of the steady state response and the synthetic steady response by studying the magnitude and phase differences were conducted. The spectral analysis showed that they both fit very well with minimal phase and magnitude differences as shown in Figure 4.19.

4.5.2 Synthetic Steady State From RAD Responses

The computation of correlation coefficient between the real and synthetic steady state responses constructed from RAD sequences (Figure 4.20) revealed high similarity at 10, 32, 50 and 68 Hz with lower percentage of correlation at 15 Hz as illustrated in Table 4.5. Moreover, frequency domain analysis of the steady state response and the synthetic steady response by studying the magnitude and phase differences were conducted. The spectral analysis showed that they both fit very well with minimal phase and magnitude differences as shown in Figure 4.21.

Table 4.5: The Correlation Coefficient Between Real Steady State and Synthetic Steady State Constructed From RAD Sequences

Rate (Hz)	Mean rate (Hz)	Correlation coefficient
2	1.95	N/A
10	10.00	0.96
15	15.03	0.86
32	31.25	0.97
50	50.00	0.92
68	68.98	0.92

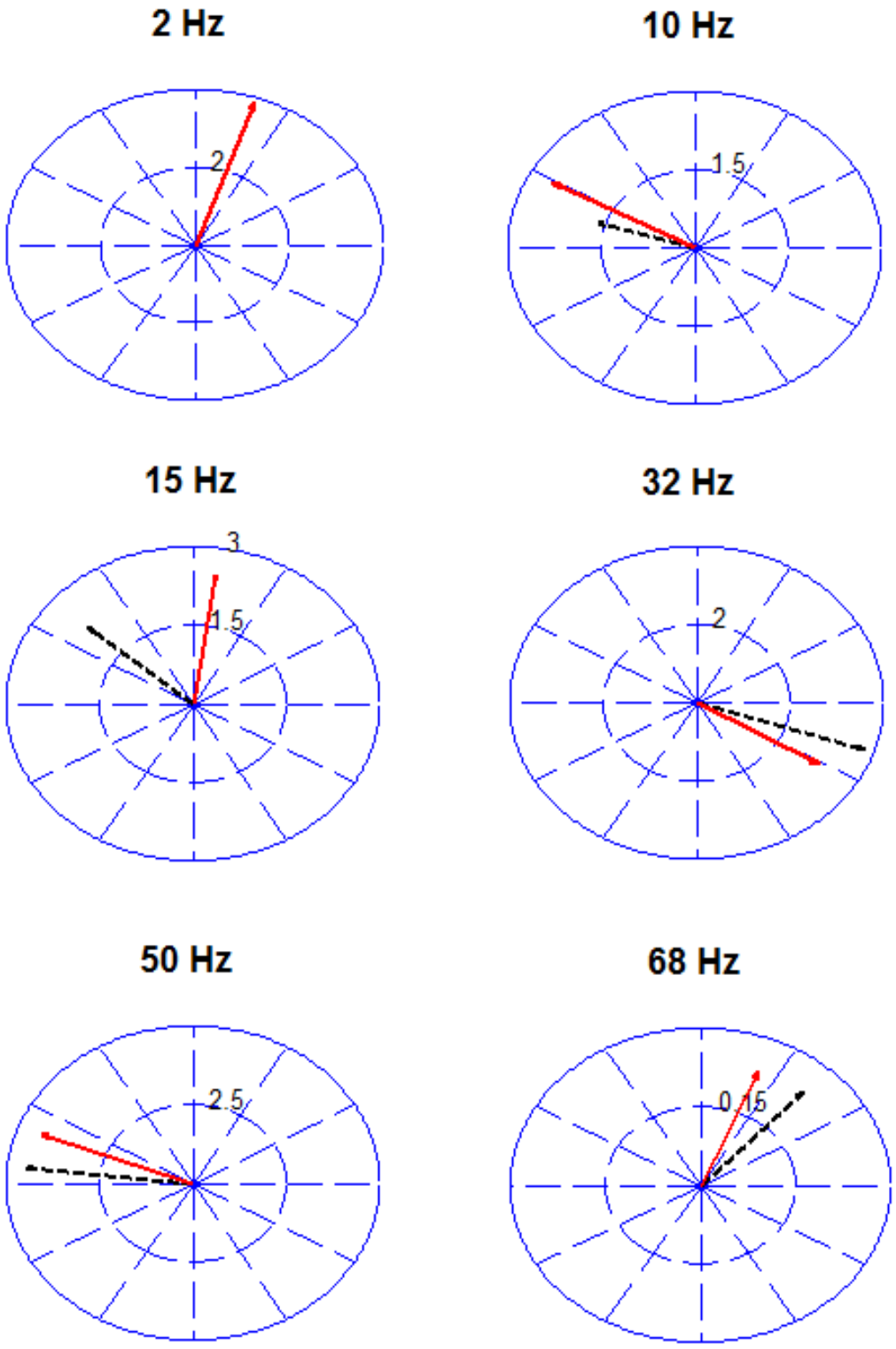

Figure 4.21: Phasor of the fundamental frequency showing the comparison of magnitudes and phases between the real steady state (black-dotted arrows) and synthetic steady state responses constructed from RAD sequences (red arrows).

Chapter 5

Summary and Discussion

This study aimed to investigate the ability to extract the per stimulus FERG response from the overlapped evoked potential at high stimulation rates of 10, 15, 32, 50 and 68 Hz using CLAD and RAD mathematical theories. In addition, the real steady state responses were acquired at the same stimulation rates using isochronic stimulation sequences. Moreover, in order to validate the extracted per stimulus FERG responses, simulation technique was used to construct the synthetic steady state responses from the specially designed QSS and RAD sequences.

In this study, the investigation of the ERG morphology with rate changes was initiated by acquiring the standard transient response. This transient response was obtained at the rate of 2 Hz by using an isochronic sequence from all the subjects to be used as a control in this study (see Figure 4.1). All the components of a transient ERG response were clearly identifiable as described in the International Society for Clinical Electrophysiology of Vision (Marmor et al., 2009). Furthermore, we examined the ability of extracting the per stimulus FERG response when high rate stimulus of 10,15,32,50 and 68 Hz are used by using the slightly jittered CLAD and RAD responses as described in section 3.2.

The transient and steady state responses obtained in this study were consistent with the existing literature (Birch & Anderson, 1992; Papathanasiou & Papacostas, 2008; Parvaresh et al., 2009). Both CLAD and RAD methods enabled a successful extraction of the “per stimulus” transient ERG responses. For the first time, it was possible to analyze the ERG responses accurately in time domain at high frequency rates in a normal population. The a-wave and b-wave amplitudes and implicit times were clearly visible in

the extracted transient responses at all stimulation rates. The experimental results showed that, as the stimulation rate increased, the a-wave and b-wave amplitudes decreased significantly between the 10 and 15 Hz and 15 and 32 Hz. Furthermore, the implicit time of a-wave increased between 2 and 10 Hz and decreased between 15 and 32 Hz. Moreover, b-wave decreased significantly as the stimulation rate increased up to 32 Hz as shown in Figure (4.9, 4.16).

Interestingly, this study revealed new high-rate morphology of FERG waveform having a positive peak that follows b-wave and lasts for about 50 ms (Figure 5.1). This peak was consistent across all stimulation rates but stronger at 32Hz. The generators of this new peak need to be investigated in future studies.

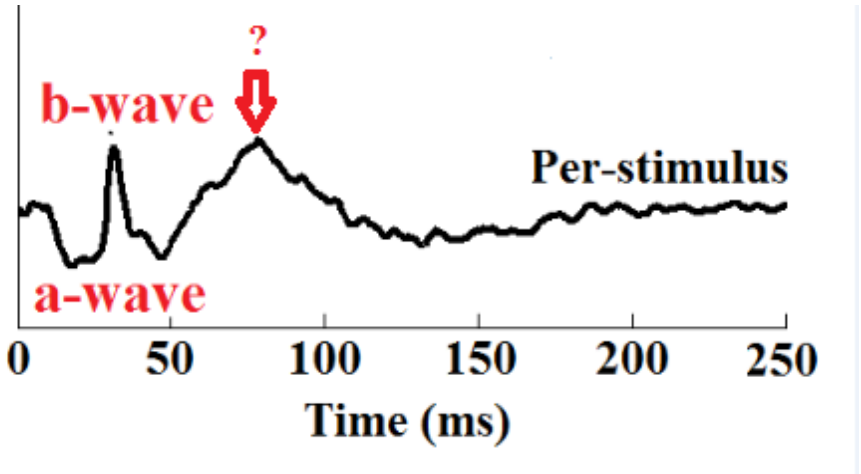

Figure 5.1: The population averaged deconvolved transient FERG at 32 Hz. A positive peak that arises at around 80 ms occurring after the b-wave was consistently observed in all subjects.

The CLAD and RAD methods assume equal "per-stimulus" unit responses for each individual stimulus in the sequence. It is not possible to predict a-priori if this assumption will hold for the evoked responses and sequences used in this study. Excessive jitter may evoke different per-stimulus responses producing an unreliable deconvolved signal. Since the extracted per-stimulus responses used in this study

successfully predicted the real recorded steady state responses, we can infer that the sequence jitter was adequate for this type of neural activity as shown in Figures (4.19, 4.21). Moreover, the temporal analysis using correlation coefficient between the real and synthetic steady state responses showed high similarity at 10, 15, 32, and 50 Hz with lower percentage of correlation at 68 Hz for synthetic steady state responses constructed from QSS sequences (see Table 4.4). On the other hand, for synthetic steady state responses constructed from RAD sequences, the correlation coefficient between the real and synthetic steady state responses showed high similarity at 10, 32, 50 and 68 Hz with lower percentage of correlation at 15 Hz (see Table 4.5). However, based on the results comparisons that used the correlation coefficients in time domain and phasor analysis in frequency domain, we can conclude that between RAD and CLAD, CLAD sequences are providing more accurate deconvolved transient responses due to the advantage of precise sequence design method.

In comparison to other studies have been conducted on ERG responses, our results showed high response consistency. However, there are amplitude differences in the waveform amplitudes that might be caused by different factors. The type of the electrodes used to measure the electrical potential has substantial effect on the responses amplitudes. Although the surface electrodes used in this study for the ease of use and subjects' comfort, there is a great reduction in the measured responses amplitude in compared with other types of electrodes that showed higher amplitudes such as, contact lens electrodes, JET, C-glide, and DTL respectively (Esakowitz et al., 1993). Nevertheless, the feasibility of using surface skin electrode with no pupil dilation has been demonstrated for clinical use (Papathanasiou & Papacostas, 2008).

In Papathanasiou and Papacostas (2008), they tested the ability to acquire the transient response of FERG at 1 Hz and the standard 30 Hz response. The b- wave average implicit time of FERG response at 1 Hz was 34.1 ms with average amplitude of 56.4 μV. Also, the a- wave average implicit time of the transient response at 1 Hz was 20.9 ms. For the standard flickering FERG, The b- wave average implicit time was 30 ms with average amplitude of 31.9 μv. thus, in comparison with the computed temporal analysis of our results, the b-wave average implicit times for CLAD and RAD were 30.53 and 31.58 respectively at 32 Hz stimulation rate.

Moreover, it has been shown that the stimuli strength has substantial effect on FERG responses. The increasing of stimuli strength leads to an increase in the responses amplitude (Binns et al., 2011). The ISCEV recommended standard stimulus strength for photopic FERG responses is 3.0 $cd \cdot s \cdot m^{-2}$ (Marmor et al., 2009). As a result, using stimulus strength of 1.5 $cd \cdot s \cdot m^{-2}$ in this study might be the reason of having lower waveforms amplitude compared with other laboratories reported results (Binns et al., 2011; Papathanasiou & Papacostas, 2008). To demonstrate that, we conducted one trial of the experiment using different LED VDU with higher stimulus intensity. The 2 Hz transient response and quasi steady state responses were acquired at rates of 10, 15, 32, 50 and 68 Hz using QSS sequences. The comparison of the conventional and deconvolved transient responses between the two VDUs showed a significant increase in the FERG responses amplitude acquired using higher stimulus strength as shown in Figure (5.2).

5.1 Future Directions

The ability of analyzing the FERG responses accurately in time domain at high frequency rates provides more information. Conducting the study on larger normal

population can be beneficial in initiating standard normal values for the FERG response component. Moreover, it is suggested to extend this study by investigating the temporal changes on patients. Thus, that can set the stage for a potential accurate retinal diagnostic tool.

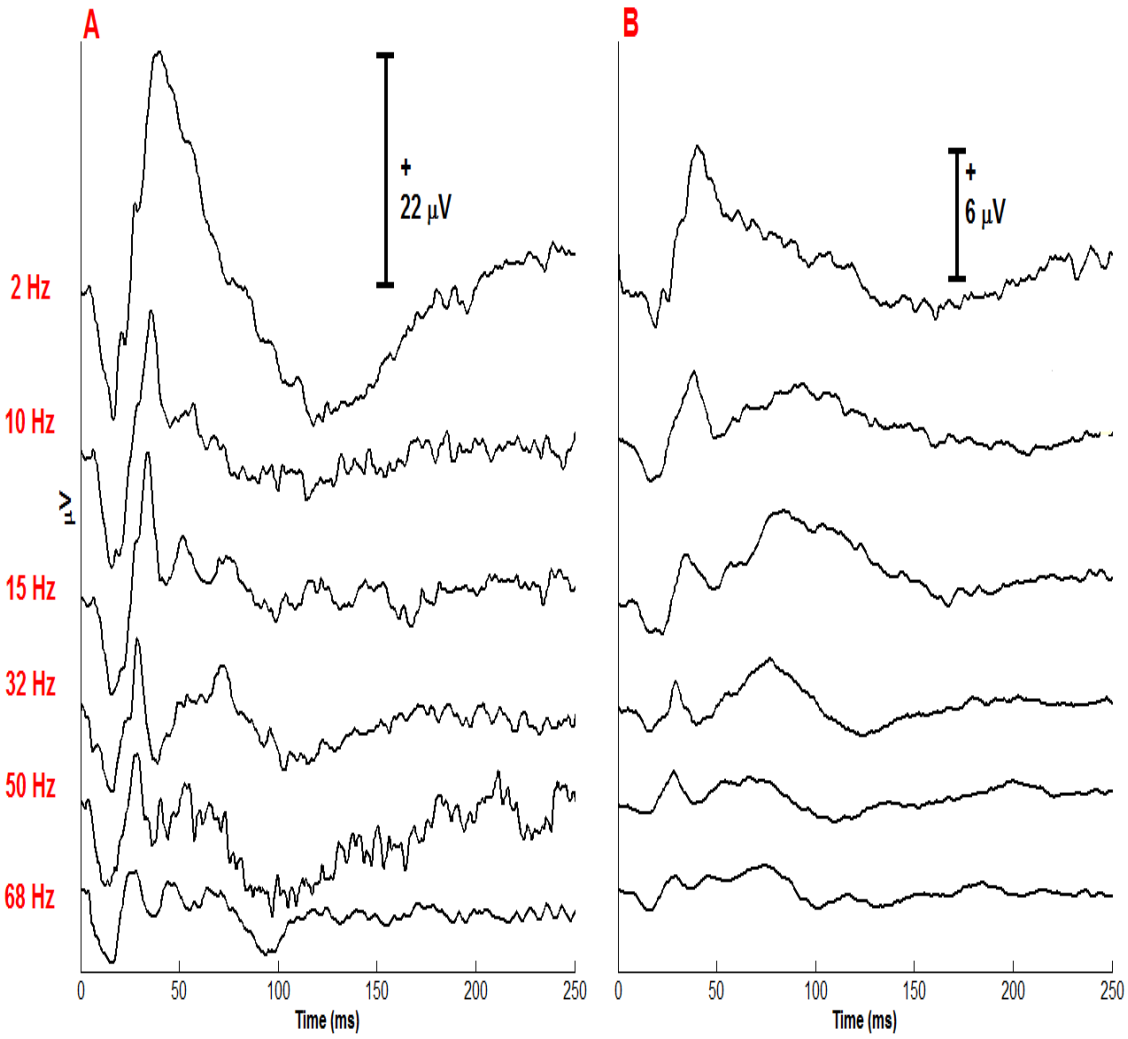

Figure 5.2: (A) One trial of FERG responses for one subject acquired by QSS sequences using higher stimulus strength and (B) Averaged three trials of FERG responses of the same subject using stimulus strength of 1.5 cd·s·m^{-2}. The responses were acquired at 2, 10,15,32,50 and 68 Hz are shown respectively.

REFERENCES

Asi, H., & Perlman, I. (1992). Relationships between the electroretinogram a-wave, b-wave and oscillatory potentials and their application to clinical diagnosis. *Documenta Ophthalmologica*, *79*(2), 125–139.

Bach, M., Brigell, M. G., Hawlina, M., Holder, G. E., Johnson, M. A., McCulloch, D. L., & Viswanathan, S. (2013). ISCEV standard for clinical pattern electroretinography (PERG): 2012 update. *Documenta Ophthalmologica*, *126*(1), 1–7.

Bach, M., & Hoffman, M.B. (2006). The origin of the pattern electroretinogram. In Heckenlively, J. R. and Arden, G. B. (Eds.), *Principles and practice of clinical electrophysiology of vision* (pp.185–196). Cambridge, MA: MIT Press.

Bardy, F., Dillon, H., & Van Dun, B. (2014). Least-squares deconvolution of evoked potentials and sequence optimization for multiple stimuli under low-jitter conditions. *Clinical Neurophysiology*, *125*(4), 727–737.

Bear, M. F., Connors, B. W., & Paradiso, M. A. (2007). *Neuroscience exploring the brain*. Baltimore, MD: Lipppincott, Williams, & Wilkins.

Binns, A. M., Mortlock, K. E., & North, R. V. (2011). The relationship between stimulus intensity and response amplitude for the photopic negative response of the flash electroretinogram. *Documenta Ophthalmologica*, *122*(1), 39–52.

Birch, D. G. (2006). Flicker electroretinography. In Heckenlively, J. R., & Arden, G. B. (Eds.), *Principles and practice of clinical electrophysiology of vision* (pp. 581–583). Baltimore, MD: Lipppincott, Williams, & Wilkins.

Birch, D. G., & Anderson, J. L. (1992). Standardized full-field electroretinography: Normal values and their variation with age. *Archives of Ophthalmology*, *110*(11), 1571–1576.

Bohórquez, J. (2006). *Deconvolution of overlapping evoked responses elicited by arbitrary stimulating sequences*. Neurosensory laboratory internal report.

Bohórquez, J., & Özdamar, Ö. (2008). Generation of the 40-Hz auditory steady-state response (ASSR) explained using convolution. *Clinical Neurophysiology*, *119*(11), 2598–2607.

Delgado, R. E., & Ozdamar, O. (2004). Deconvolution of evoked responses obtained at high stimulus rates. *Journal of the Acoustical Society of America*, *115*(3), 1242–1251.

Esakowitz, L., Kriss, A., & Shawkat, F. (1993). A comparison of flash electroretinograms recorded from Burian Allen, JET, C-glide, gold foil, DTL and skin electrodes. *Eye*, *7*(1), 169–171.

Frishman, L.J. (2006). Origins of the electroretinogram. In Heckenlively, J. R., & Arden, G. B. (Eds.), *Principles and practice of clinical electrophysiology of vision* (pp. 139–183). Cambridge, MA: MIT Press.

Gauras, P. (1970). Electroretinography: Some basic principles. *Investigative Ophthalmology*, *9*(8), 557–569.

Gundogan, F. C., Tas, A., & Sobaci, G. (2011). Electroretinogram in hereditary retinal disorders. In Dr. Gregor Belusi (Ed.), *Electroretinograms* (95–132). Croatia: InTech.

Harden, A., Adams, G. G., & Taylor, D. S. (1989). The electroretinogram. *Archives of Disease in Childhood*, *64*(7), 1080–1087.

Heckenlively, J. R., Weleber, R. G., & Arden, G. B. (2006). Testing levels of the visual system. In Heckenlively, J. R., & Arden, G. B. (Eds.), *Principles and practice of clinical electrophysiology of vision* (pp. 623–630). Cambridge, MA: MIT Press.

Heinrich, S. P. (2010). Some thoughts on the interpretation of steady-state evoked potentials. *Documenta Ophthalmologica*, *120*(3), 205–214.

Holder, G. E. (1987). Significance of abnormal pattern electroretinography in anterior visual pathway dysfunction. *British Journal of Ophthalmology*, *71*, 166–171.

Hood, D. C., Bach, M., Brigell, M., Keating, D., Kondo, M., Lyons, J. S., . . ., & Palmowski-Wolfe, A. M. (2012). ISCEV standard for clinical multifocal electroretinography (mfERG) (2011 edition). *Documenta Ophthalmologica*, *124*(1), 1–13.

Hung, G. K., & Ciuffreda, K. J. (2002). *Models of the visual system*. New York, NY: Kluwer Academic.

Kim, H. D., Park, J. Y., & Ohn, Y. H. (2010). Clinical applications of photopic negative response (PhNR) for the treatment of glaucoma and diabetic retinopathy. *Korean Journal of Ophthalmology*, *24*(2), 89–95.

Kolb, H., Fernandez, E., & Nelson, R. (2007). *Webvision: The organization of the retina and visual system.* Bethesda, MD: National Library of Medicine. Retrieved from http://webvision.med.utah.edu

Marieb, E. N. (2006). *Essentials of human anatomy & physiology*. San Francisco, CA: Pearson.

Marmor, M. F., Holder, G. E., Porciatti, V., Trick, G. L., & Zrenner, E. (1995). Guidelines for basic pattern electroretinography. *Documenta Ophthalmologica*, *91*(4), 291–298.

Marmor, M. F., Holder, G. E., Seeliger, M. W., & Yamamoto, S. (2004). Standard for clinical electroretinography (2004 update). *Documenta Ophthalmologica*, *108*, 107–114.

Marmor, M. F., Fulton, A. B., Holder, G. E., Miyake, Y., Brigell, M., & Bach, M. (2009). ISCEV Standard for full-field clinical electroretinography (2008 update). *Documenta Ophthalmologica*, *118*(1), 69–77.

Niemeyer, G. (2004). Das Elektroretinogramm: Nützlich und nicht kompliziert.*Ophta Schweizer. Fachzeitschrift Augenärztliche Medizin*, *5*, 7–13.

Niemeyer, G., & Stähli, P. (1996). ERG-diagnose und differential diagnose: Untersuchungsergebnisse über 6 Jahre. *Klinische Monatsblätter für Augenheilkunde*, *208*(05), 306–310.

Niemeyer, G. (2001). Retinal research using the perfused mammalian eye. *Progress in Retinal and Eye Research*, *20*(3), 289–318.

Özdamar, Ö., & Bohórquez, J. (2006). Signal-to-noise ratio and frequency analysis of continuous loop averaging deconvolution (CLAD) of overlapping evoked potentials. *Journal of the Acoustical Society of America*, *119*(1), 429–438.

Papathanasiou, E. S., & Papacostas, S. S. (2008). Flash electroretinography: Normative values with surface skin electrodes and no pupil dilation using a standard stimulation protocol. *Documenta Ophthalmologica*, *116*(1), 61–73.

Parvaresh, M. M., Ghiasian, L., Falavarjani, K. G., Sanjari, M. S., & Sadighi, N. (2009). Normal values of standard full field electroretinography in an Iranian population. *Journal of Ophthalmic and Vision Research*, *4*(2), 97–101.

Poppele, R. E., & Maffei, L. (1967). Frequency analysis of the electroretinogram. *Journal of Neurophysiology*, *30*(5), 982–992.

Porciatti, V., Bosse, B., Parekh, P. K., Shif, O. A., Feuer, W. J., & Ventura, L. M. (2013). Adaptation of the Steady-state PERG in Early Glaucoma. *Journal of Glaucoma*.

Porciatti, V., & Ventura, L. M. (2004). Normative data for a user-friendly paradigm for pattern electroretinogram recording. *Ophthalmology*, *111*(1), 161–168.

Porciatti, V., & Ventura, L. M. (2009). Physiological significance of steady-state PERG losses in glaucoma: Clues from simulation of abnormalities in normal subjects. *Journal of Glaucoma*, *18*(7), 535–542.

Porciatti, V., Falsini, B., Brunori, S., Colotto, A., & Moretti, G. (1987). Pattern electroretinogram as a function of spatial frequency in ocular hypertension and early glaucoma. *Documenta Ophthalmologica*, *65*(3), 349–355.

Prasad, S., & Galetta, S. L. (2011). Anatomy and physiology of the afferent visual system. *Handb Clin Neurol*, *102*, 3–19.

Remington, L. A. (2012). *Clinical anatomy and physiology of the visual system*. St. Louis, MO: Elsevier.

Roberts, A. M. (2010). *The complete human body*. New York, NY: DK.

Rogers, K. (Ed.). (2011). *The human body: The eye: The physiology of human perception.* New York, NY: Britannica Educational.

Toft-Nielsen, J. A. (2012), *Acquisition and analysis of high rate pattern electroretinograms* (Doctoral dissertation). Retrieved from Open Access Dissertations. (No. 847)

Toft-Nielsen, J., Bohorquez, J., & Ozdamar, O. (2011). Innovative pattern reversal displays for visual electrophysiological studies. *Proceedings of the Engineering in Medicine and Biology Society, 2011*, 2009–2012.

Toft-Nielsen, J., Bohórquez, J., & Özdamar, Ö. (in press). Unwrapping of transient responses from high rate overlapping pattern electroretinograms by deconvolution. *Clinical Neurophysiology*.

Valderrama, J. T., Alvarez, I., de la Torre, A., Segura, J. C., Sainz, M., & Vargas, J. L. (2012). Recording of auditory brainstem response at high stimulation rates using randomized stimulation and averaging. *Journal of the Acoustical Society of America*, *132*(6), 3856–3865.

Ventura, L. M., Porciatti, V., Ishida, K., Feuer, W. J., & Parrish II, R. K. (2005). Pattern electroretinogram abnormality and glaucoma. *Ophthalmology*, *112*(1), 10–19.